Alkylphenol inverse agonists of HCN1 gating: H-bond propensity, ring saturation and adduct geometry differentially determine efficacy and potency

Rebecca L Joyce[1], **Nicole P Beyer**[1], **Georgia Vasilopoulos**[1], **Kellie A. Woll**[3], **Adam C Hall**[2], **Roderic G Eckenhoff**[3], **Dipti N Barman**[1], **J David Warren**[1], **Gareth R Tibbs**[1], and **Peter A Goldstein**[1]

[1]Weill Cornell Medicine, New York, NY,

[2]Smith College, Northampton, MA,

[3]University of Pennsylvania Perelman School of Medicine, Philadelphia, PA

Abstract

Background and purpose—In models of neuropathic pain, inhibition of HCN1 is anti-hyperalgesic. 2,6-di-*iso*-propyl phenol (propofol) and its non-anesthetic congener, 2,6-di-*tert*-butyl phenol, inhibit HCN1 channels by stabilizing closed state(s).

Experimental approach—Using *in vitro* electrophysiology and kinetic modeling, we systematically explore the contribution of ligand architecture to alkylphenol-channel coupling.

Key results—When corrected for changes in hydrophobicity (and propensity for intra-membrane partitioning), the decrease in potency upon 1-position substitution (NCO~OH >> SH >>> F) mirrors the ligands' H-bond acceptor (NCO > OH > SH >>> F) but not donor profile (OH > SH >>> NCO~F). H-bond elimination (OH to F) corresponds to a $\Delta\Delta$G of ~4.5 kCal mol^{-1} loss of potency with little or no disruption of efficacy. Substitution of compact alkyl groups (*iso*-propyl, *tert*-butyl) with shorter (ethyl, methyl) or more extended (*sec*-butyl) adducts disrupts both potency and efficacy. Ring saturation (with the obligate loss of both planarity and π electrons) primarily disrupts efficacy.

Conflicts of Interest

PAG and GRT are co-inventors on patents related to the development of alkylphenols for the treatment of neuropathic pain and serve on the Scientific Advisory Board for Akelos, Inc., a research-based biotechnology company that has secured a licensing agreement for the use of those patents.

Conclusions and implications—A hydrophobicity-independent decrement in potency at higher volumes suggests the alkylbenzene site has a volume of 800 Å³. Within this, a relatively static (with respect to ligand) H-bond donor contributes to initial binding with little involvement in generation of coupling energy. The influence of π electrons/ring planarity and alkyl adducts on efficacy reveals these aspects of the ligand present towards a face of the channel that undergoes structural changes during opening. The site's characteristics suggest it is "druggable"; introduction of other adducts on the ring may generate higher potency inverse agonists.

Graphical Abstract
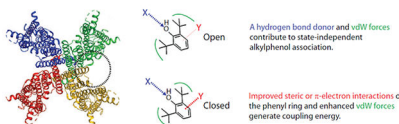
Keywords

HCN channels; inverse agonists; kinetic modeling; Neuropathic pain; anti-hyperalgesia; propofol; alkylphenol; cyclohexanol; phenyl-isocyanate; phenyl-thiol; phenyl-fluorine; 2-fluoro-1; 3-di-*iso*propylbenzene

1. Introduction

Neuropathic pain is pain caused by a lesion of, or damage to, the somatosensory nervous system [1, 2]. Neuropathic pain is a pathologic feature of numerous conditions, including postherpetic neuralgia, trigeminal neuralgia, sensory (painful) radiculopathy, painful diabetic neuropathy, peripheral nerve injury, stroke, and treatment with antineoplastics [2–4]. Globally, it is estimated that 7– 10% of the population lives with chronic pain with neuropathic features [2–6]. Cardinal symptoms of neuropathic pain are spontaneous pain, abnormal response to non-painful (allodynia) or painful (hyperalgesia) stimuli, dysesthesia (unpleasant/strange sensation – "tingling" "pins and needles"), and enhanced thermal sensitivity; numerous pharmacologic approaches to relieving neuropathic pain have been proposed [3], but their efficacy is limited, resulting in a large unmet need with respect to providing meaningful pain relief [7].

Recent work suggests that neuropathic pain might better be understood at the mechanistic level as a function of sensory profiling rather than disease etiology [8]. Hyperexcitability of primary afferent neurons is thought to be an early causal factor leading to the development and maintenance of peripheral neuropathic pain [1, 9]. Numerous ion channel families contribute to this hyperexcitability, including the hyperpolarization-activated, cyclic nucleotide-gated (HCN) channel family [10]. In animal models of neuropathic pain, non-selective HCN block with either ZD7288 [11–14] or the clinically-available drug ivabradine [15–17] results in significant anti-hyperalgesia. HCN1 expression is upregulated in multiple animal models of neuropathic pain including those wherein the initiating injury was mechanical damage [11–13], chemotherapy administration [16–19], or diabetes [20]. Anti-hyperalgesic activity is retained in HCN1-selective molecules [21–24], suggesting that HCN1-selective blockade has therapeutic potential.

Previously we demonstrated that the intravenous general anesthetic 2,6-di-*iso*-propyl phenol (propofol, DIP-P) and its closely related, non-anesthetic congener 2,6-di-*tert*-butyl phenol (DTB-P), were HCN1-selective inhibitors of channel gating [22, 25]. Such inhibition resulted from ligand-mediated stabilization of channel closed state(s), which was solely dependent upon interactions with the membrane embedded channel core [25]. Both DIP-P and DTB-P provided mechanical and thermal anti-hyperalgesia in mouse peripheral nerve injury neuropathic pain models [22, 23].

In silico modelling and crystallography demonstrate alkylphenols dock in cavities in $GABA_A$ receptors ($GABA_A$-Rs) [26, 27] where they likely displace either native acyl chains [28] or water [29–31]. Crystallography further reveals acyl chains associate with, and intercalate between, the voltage sensor and pore domains of K_v channels, indicating specific packing at the lipid-channel interface is thermodynamically favored [32]. Given the structural homology between HCN1 and K_v channels [10, 33], we posit that specific acyl (and water) filled cavities are also present on HCN channels. Consequently, the HCN1-alkylphenol association is likely similar in nature, but likely unique in detail, to the alkylphenol interaction with $GABA_A$-Rs, and that the alkylphenol:HCN1 association can be defined and optimized.

In the present study, we demonstrate that H-bonding, ring planarity and/or π electron interactions and coupling to ring adducts at the 2 and 6 positions all contribute to HCN1 inhibition at a site with a volume 800 $Å^3$. Such characteristics are consistent with alkylphenols acting at a defined site within the membrane-embedded core of HCN1 channels. Examination of HCN sequences in conjunction with the cryo-EM structure of HCN1, shows multiple sites of divergence within this region. Together, the data suggest that alkylphenol-mediated inhibition of HCN1 channel opening occurs *via* a defined and "druggable" site which, if correct, may open the way to generation of a novel class of high-potency, non-opioid, therapeutics for neuropathic pain.

2. Materials and Methods

2.1 Molecular Biology

Methods for heterologous expression were as previously described [22]. Briefly, cDNA encoding murine HCN1 channels were sub-cloned into a pGH19 vector and amplified in STBL2 cells (Invitrogen Corporation, Grand Island, NY, USA). cRNA was transcribed from NheI linearized DNA using T7 RNA polymerase (Message Machine; Ambion, Houston, TX, USA).

2.2 Electrophysiology

Recordings were made from *Xenopus* oocytes (Ecocyte, Austin, TX) 1–3 days after cRNA injection (1–50 ng/oocyte). Cells were maintained in L-15 media without Ficoll (Specialty Media, Phillipsburg, NJ) at 16 °C until use.

Two-electrode voltage clamp (TEVC) data were acquired using a Warner Instruments (Hamden, CT) OC-725C amplifier, filtered at 1 kHz (Frequency Devices Bessel model 902, Ottawa, IL) digitized at 2 kHz by an ITC-18 interface (Instrutech Corporation, Port

Washington, NY) and recorded with Pulse software (HEKA Elektronik, Lambrecht/Pfalz, Germany).

Microelectrodes were fabricated from 1B120-F4 borosilicate glass (World Precision Instruments, Sarasota, FL) and had resistances of $0.1 – 0.5$ MΩ (I passing) and $1 – 4$ MΩ (V sensing) when filled with 3 M KCl. An active virtual ground was used to clamp the bath. Ag-AgCl ground wire(s) were connected to the bath solution by 3 M KCl-2% agar salt bridges placed downstream of, but close to, the oocyte. Oocytes were bathed in a recording solution of (in mM): 107 NaCl, 5 KCl, 1 $CaCl_2$, 1 $MgCl_2$, 10 HEPES-free acid pH 7.4 (NaOH). Recordings were obtained at room temperature. In all cases, voltages are reported as the command potentials. The observed potential was within 1% of the command.

2.3   Paradigms and analysis

The holding potential was −30 mV. Tail currents were recorded at 0 mV. Steady-state activation properties were determined from tail current activation curves (see Riegelhaupt *et al.* for a discussion on the criteria adopted to eliminate collection and analysis bias - [34]). Fits of these relations with the Boltzmann function (equation 1 where A_1 is the current offset and A_2 the maximal amplitude and V the step voltage) yielded the $V_{1/2}$ (the activation mid-point) and the slope factor (equal to RT/ZF where R, T and F have their usual meaning and Z is an approximation of the gating charge associated with activation).

$$I(V) = A_1 + A_2 / \left\{ 1 + e^{\frac{ZF(V - V_{1/2})}{RT}} \right\} \quad 1.$$

Gating of HCN channels is slowed in the presence of in the presence of inverse agonists. To ensure the determined Boltzmann parameters reflect thermodynamic behavior free of kinetic contamination, we routinely determined the gating parameters using step durations of 3 s and 5 s. In no case was there a systematic difference in fit parameters. This observation is consistent with activation being equilibrated at all voltages under all conditions tested. The two determinations were averaged and treated as a single measurement. Data reported as shifts in the $V_{1/2}$ ($V_{1/2}$) were determined with respect to vehicle control recordings performed before and after the experimental determinations. Standard errors around vehicle populations were less than 1 mV.

Concentration response data were fit with the Hill equation (equation 2), where $V_{1/2}$ is as defined above, $V_{1/2}$ max the maximal change as determined from the fit, IC_{50} the concentration of ligand required for half maximal inhibition of gating and h the Hill coefficient. In all fits, $V_{1/2}$ in the absence of ligand was constrained to zero. For several ligands, estimates of IC_{50} were determined assuming $V_{1/2\ max}$ and h were equal to those obtained for DTB-P (see thin green lines on Figure 3 and discussion thereof).

$$\Delta V_{1/2} = \Delta V_{1/2\,max} / \left\{ 1 + \left(\frac{IC50}{[\text{ligand}]} \right)^{h} \right\} \quad 2.$$

2.4 Modeling of alkylphenol and alkylcyclohexanol coupling to channel gating

To consider the mechanistic basis by which chemical modification(s) of the alkylphenol structure perturbs coupling of the ligands to HCN1, we examined models of the form shown schematically in Figure 1.

Here, C_R, C_A and O represent the closed-resting, closed-activated and open states, of the channel. L is the voltage independent equilibrium constant that describes opening of activated channels. Activation of voltage sensors is described by the voltage-dependent equilibrium constant K_V (equation 3) where K_V^0 is K_V in the absence of an applied field.

$$K_V = K_V^0 / e^{\frac{ZFV}{RT}} \quad 3.$$

I and H are full and partial inverse agonists, respectively. Consistent with previous work wherein we showed DIP-P was indifferent to the activation status of the voltage sensors [25], here we assume neither I nor H alter K_V. Which is to say both I and H are considered to bind equally well (or poorly) to C_R and C_A. I binds tightly to C_R and C_A (as defined by the association constant K_C^I) but poorly to O (as defined by the association constant K_O^I) and thus acts as a full inverse agonist of opening. For the partial inverse agonist, H, the loss of efficacy must arise from proportionally weaker binding to C than to O when compared to binding of I. While it is critical to understand how such partial behavior arises, particularly when considering rational drug design, it is not possible to *a priori* intuit whether it arises due to a loss of function (a proportionally greater decrement in K_C versus K_O) or a gain of function (a proportionally greater improvement in K_O versus K_C).

Within this overall scheme, we examined two limiting conditions. Specifically, we assumed I and H bind to common site(s) or to distinct site(s). Here, the definition of common site(s) includes pocket(s) with over-lapping structures, occupancy of which are mutually-exclusive. In contrast, distinct sites are, *de facto*, non-overlapping. In the common site model, the sum of p and q cannot exceed S (where p and q represent the number of binding events of I and H, respectively, and S is the number of sites *per* channel) and the equation determining the change in the $V_{1/2}$ ($\Delta V_{1/2}$) due to the presence of I and/or H is given by equation 4. In the distinct site model, p and q can both equal S and $\Delta V_{1/2}$ is given by equation 5.

$$\Delta V_{1/2}(H/I) = \frac{RT}{ZF} * \ln \frac{1 + L * \left\{ \frac{1 + A + B}{1 + C + D} \right\}^{S}}{1 + L} \quad 4.$$

$$\Delta V_{1/2}(H/I) = \frac{RT}{ZF} * \ln \frac{1 + L * \left\{ \frac{(1+A)(1+B)}{(1+C)(1+D)} \right\}^{S}}{1 + L} \qquad 5.$$

In both equations, $A = [H]*K_O^H$, $B = [I]*K_O^I$, $C = [H]*K_C^H$ and $D = [I]*K_C^I$. Note that in the presence of only H or I (and the absence of both) equations 4 and 5 become equivalent. It is the behavior of gating in the combined presence of H and I that distinguishes between these two mechanisms.

To allow us to simultaneously fit the behavior of *iso*-propyl and *tert*-butyl analogues, we defined two sets of equilibrium constants wherein K_O^H, K_O^I, K_C^H and K_C^I describe *tert*-butyl association and Q_O^H, Q_O^I, Q_C^H and Q_C^I describe *iso*-propyl association. Versions of equations 4 and 5 describing individual ligand effects and additivity were generated by substitution of the appropriate equilibrium constants (and corresponding ligand concentration terms). In simultaneous fits to the *iso*-propyl and *tert*-butyl data, all eight binding constants and L were free parameters. Importantly, equations 4 and 5 show that the degrees of freedom in the common and distinct site models are identical and that this is independent of S. As such, measures of the goodness of fit are directly comparable. As is evident from inspection of equations 4 and 5, in models where inhibitors do not discriminate between C_R and C_A, K_V does not contribute to their influence on $V_{1/2}$.

We applied only three constraints. First, S (the number of sites *per* channel), was held to be either 1 or 4. While arbitrary, this is consistent with the tetrameric nature of HCN channels. An S of 1 is consistent with the site being at the four-fold axis of symmetry, that is, at a point of juxtaposition of all four subunits. An S of 4 is consistent with the sites lying within or between channel subunits and distant (with respect to ligand size) from the central axis. Second, the gating valence Z was held equal to 2.82. This value was determined from fits of the Boltzmann function to control GV relations. While not arbitrary, it is well understood that, in a complex system such as exists for HCN gating, the slope of such a fit is a secondary, and imprecise, measure that will likely underestimate the total charge moved [35, 36]. However, given that our three-state gating scheme is a clear simplification in and of itself ([37] and references therein) and in the model Z serves only as a proportionality term (equations 4 and 5), an error in the estimation of Z will have no impact on the qualitative integrity of our analysis (assuming Z is constant). Is an assumption of constancy of Z reasonable? At high concentrations, DIP-P and DTB-P both decrease the steepness of the gating relation (*i.e.*, the Boltzmann slope term gets larger, meaning the estimated value of Z would get smaller – not shown). Would use of experimentally determined values of Z under each condition be better? We think not; while a change in the GV slope could imply Z has changed, it is highly improbable that the fundamental motions of the sensors (and of the net charge moved) is radically altered by the presence of an alkylbenzene. A more reasonable interpretation of changes in the activation slope is that this reflects altered co-operativity between subunits, an effect the Boltzmann equation does not account for. For these reasons, we consider use of a stable measure of charge moved to be the conservative assumption.

Third, and finally, values of all equilibrium constants were constrained to be >0, a physically reasonable expectation.

To examine the secondary butyl analogue of DTB-P (2,6-di-*sec*-butyl phenol; DSB-P) we defined a third set of equilibrium constants, J_O and J_C. As responses to the DSB-P were only observed at high concentrations and were, therefore, relatively poorly determined, these data were not included in the simultaneous fit of *iso*-propyl and *tert*-butyl responses as *per* Figure 5. For the DSB-P fit, all parameters other than J_O and J_C were held equal to the values used and/or determined for and from the fits shown in Figure 5 and reported in Table 4.

Association constants determined from the fits of the models were transformed to free energy terms according to equation 6.

$$\Delta G = -RT \ln K \quad 6.$$

It is important to note that within both classes of models the maximal $V_{1/2}$ is limited to $RT/ZF * \ln 1/1+L$ (equations 4 and 5) and, *ipso facto*, the maximal observed response of the most effective inverse agonist will strongly influence the estimate of L. This arises because the inverse agonists are stabilizing closing and, therefore, can only register an inhibitory voltage shift to the extent permitted by opposing the effect of a favorable opening transition (large L) that normally drags the activation transition forward. What does this mean with respect to the behavior expected within competition experiments? Intuitively, for a channel behaving according to the common site model, the main phenotype will be for the partial inverse agonist to have no effect in the face of an intermediate concentration of the full inverse agonist (or suppress that if high enough concentrations of the partial inverse agonist can be achieved and its maximal response is lower than that of the included concentration of full inverse agonist). In contrast, while the actions of partial and full inverse agonists acting via distinct sites will be (as expected) energetically additive, this will only be revealed as an additive effect on the $V_{1/2}$ at sub-maximal concentrations of the full inverse agonist. Together, these considerations reveal examination of ligands of unknown properties need to be considered in the face of a low concentration of DTB-P. We selected 3 μM.

Theoretically, an independent measure of L can be determined from the maximal open probability (P_{MAX}). While conceptually straightforward, determining P_{MAX} of HCN1 channels is difficult. First, the single channel conductance of HCN channels is very low, making direct analysis of single channel records problematic. Second, wild-type HCN1 channels cluster and gating is slow making noise analysis similarly challenging. We have previously shown that deletion of the N and C termini of HCN1 generates HCN1 channels that are amenable to non-stationary fluctuation analysis (NSFA; [25]). When determined in excised inside-out patches in high K^+ recording conditions (to maximize the current amplitude), the P_{MAX} of HCN1- Nν C is 0.88, which corresponds to a value of L of 7.3 (equation 7).

$$L = \frac{P_{MAX}}{1 - P_{MAX}} \quad 7.$$

However, it should be noted that analysis of HCN1- ΔNvΔC in the excised patch configuration as used for NSFA will underestimate the likely value of L of wtHCN1 as the effect of at least three factors that stabilize gating (internal cAMP, internal 4,5-PIP_2, and a physiological level of external Na^+ and K^+) are lost. This disruption is reflected in a 40 mV hyperpolarization of gating of HCN1 upon patch excision. If these positive regulators all acted *via* enhancing L (stabilizing opening), equation 7 reveals L would be 93-fold higher in intact cells than reported by NSFA in excised patches. Further, it is clear that while the effect of 4,5-PIP_2 seems to involve, at least in part, a surface charge contribution, the positive effects of cAMP (5–7 mV right-shift in the $V_{1/2}$ for HCN1) and physiological external Na^+ and K^+ concentrations (10–12 mV) do indeed arise from a stabilization of opening [38–41] (and our unpublished observations). Thus, the model determined value of L of 125 is completely consistent with independent experimental evidence wherein endogenous positive modulation of L accounts for 25 mV of the observed 40 mV difference between recording modes.

Equation 8 determines the value of L in an intact cell under TEVC (L_T) as a function of the value of L determined from NSFA in excised inside out patches (L_I) and $V_{(T-I)}$, the difference in $V_{1/2}$ between these modes. Equation 8 assumes K_V^0 is unaltered by patch excision.

$$L_T = \left(1 + L_I\right) * e^{\frac{ZFV(T-I)}{RT}} - 1 \quad 8.$$

2.5 Physicochemical parameter estimates

We found determinations of ligand physicochemical parameters used in this study to be sensitive to the analysis engine used (not shown but compare values in Tables 1 and 2 to those of Krasowski et al. and Woll et al. [42, 43]). To provide a unified set of values, we redetermined chemical properties using a single engine, the Maestro 2018–2 package from Schrödinger. LigPrep was used to generate all possible states at a target pH of 7.4 ± 0.2. QikProp was used to calculate the reported properties of all generated states. Properties are reported in Tables 1 (phenyl derivatives) and 2 (cyclohexanol derivatives). LogP is log of the calculated octanol/water partition coefficient. Values for all ligands in the matrix are provided to facilitate cross-study comparisons.

2.6 Data and statistical analysis

Data analysis was performed in PulseFit (HEKA Elektronik) or using custom analysis routines written in IgorPro (Wavemetrics Corporation, Lake Oswego, OR). Data were typically collected and analyzed independently by two or more experimenters with some

recordings randomly selected for independent reanalysis. Data are presented as mean ± SEM with the numbers of observations per data set reported in figure legends. Errors around Hill fit parameters and the equilibrium constants determined from fits of the gating model are non-linear regression approximations of the standard deviation.

Fits of the Hill equation were to the individual data. To minimize the effect of different population sizes on the global minimization, fits of the models were to mean behavior. As all models have the same degrees of freedom and were fit to a common data set, the goodness of fits are directly comparable and allow for robust model discrimination. A two-tailed t-test was used to compare two populations. Comparisons between multiple populations and a control were by one-way ANOVA using Dunnett's test for multiple comparisons. Statistical tests were performed in SigmaStat 4.0 (Systat Software).

2.7 Chemicals and reagents

Phenols: 2,6-di-methyl phenol (DM-P; Sigma-Aldrich Cat. # D175005), 2,6-di-ethyl phenol (DE-P; Sigma-Aldrich Cat. # CBR02039), 2,6-di-*iso*-propyl phenol (DIP-P; Sigma-Aldrich Cat. # D126608), 2,6-di-*tert*-butyl phenol (DTB-P; Sigma-Aldrich Cat. # D48400), 2,6-di-*sec*-butyl phenol (DSB-P; Acros Organics, Fairlawn, NJ, USA Cat. #AC15283).

Isocyanates: 2,6-di-methyl phenyl-isocyanate (DM-PIC; Sigma-Aldrich, Cat. # 252336), 2,6-diethyl phenyl-isocyanate (DE-PIC; Alfa Aesar, Ward Hill, MA, USA Cat. # L11339), 2,6-di-*iso*propyl phenyl-isocyanate (DIP-PIC; Sigma-Aldrich Cat. # 376930).

Thiols: 2,6-di-methyl phenyl-thiol (DM-PT; Sigma-Aldrich Cat. # 306940); 2,6-di-*iso*-propyl phenyl-thiol (DIP-PT) was synthesized within the Milstein Chemistry Core Facility at Weill Cornell Medicine. LCMS, ^{1}H-NMR, and ^{13}C-NMR analysis conformed to literature precedent [44] and confirmed purity at >99%.

Fluoro: 2-Fluoro-1,3-di-*iso*-propylbenzene was synthesized as previously described [43]. For clarity, here we use a nomenclature that accords with the other molecules studied, that is, 2,6-di-*iso*-propyl phenyl-fluorine (DIP-PF).

Cyclohexanols: 2,6-di-methyl cyclohexanol (DM-CH) was obtained from Acros Organics (Thermo Fisher Scientific, New Jersey, USA; Cat. # 149810050); 2,6-di-ethyl cyclohexanol (DE-CH), 2,6-di-*iso*-propyl cyclohexanol (DIP-CH) and 2,6-di-*sec*-butyl cyclohexanol (DSBCH) were as previously described [45]. 2,6-di-*tert*-butyl cycloxhexanol (DTB-CH) was synthesized within the Milstein Chemistry Core Facility at Weill Cornell Medicine. LCMS, ^{1}H-NMR, and ^{13}C-NMR analysis conformed to literature precedent [45] and confirmed purity at >99%.

All ligands were prepared as stock solutions in DMSO then dispersed in the bath solution with vigorous stirring for at least 60 minutes. In the absence of any other excipient, the final DMSO concentration was 0.2% ($^V/_V$). 2-Hydroxypropyl-β-cyclodextrin (HPβCD; Sigma-Aldrich, St. Louis, MO;H107) can increase the solubility of ligands such as DTB-P and DIP-P by 200-fold and do so with no effect on pharmacokinetics ([22]; and references therein). In an attempt to extend the range of the concentration responses we could examine, in some

experiments we included HPβCD. While the presence of HPβCD did not qualitatively alter the behavior of any ligand, its presence did cause a modest right-shift in the inverse agonist concentration response curves when it was included. However, as the right-shift was not demonstrably outside the normal scatter observed in the data between recordings from different donor frogs on different days and was far smaller than the variance in the model fit parameters, the different vehicle conditions were combined.

3. Results

3.1 H-bond interactions with position 1 confer potency

Figure 2 shows representative families of voltage-clamp recordings (Figure 2A) in either vehicle or vehicle plus 10 μM of one of four 2,6-di-*iso*-propyl phenyl derivatives (Figure 2B, also Figure 3). Inspection of the records suggests that systematic perturbation of the H-bonding capability of the adduct at the 1-position leads to a disruption of inhibition of HCN1 gating. This inference is confirmed by inspection of the activation curves (Figure 2C).

Diminished inhibition could be due to reduced efficacy, a weakening of potency, or both. To address this, we constructed complete concentration-response relations for the four ligands (Figure 3 central column, first four rows). Inspection confirms there is a loss of potency upon 1-position substitution. The progressive loss of potency (DIP-P > DIP-PT > DIP-PIC >>> DIP-PF) evident in Figure 3 and 4A (symbols within the dashed ellipse – see also Table 3) does not track the ability of the ligands to act as either a H-bond donor (DIP-P > DIP-PT >>> DIP-PIC ~ DIPPF) or acceptor (DIP-PIC > DIP-P > DIP-PT >>> DIP-PF) (Table 1).

It should be noted, however, that changing the 1-position adduct will alter not just the H-bonding profile of the ligand but other aspects of its physical chemistry. Thus, the four ligands here will have modestly different volumes, pKa's and markedly divergent hydrophobicities (Table 1), and each of these properties is examined below.

3.2 Compensating for partitioning reveals the 1-position adduct influences potency through action as an H-bond acceptor

Due to partitioning, at an equivalent aqueous concentration, more hydrophobic molecules will have a higher intra-plasma membrane concentration. As alkylphenols act by coupling to the membrane embedded core of HCN1 channels [25], we next asked whether partitioning *per se* alters either the rank order and/or energetic strength of 1-position adduct substitutions.

To address this, we assumed the within-membrane concentration of each ligand at its aqueous IC_{50} can be represented by the aqueous IC_{50} multiplied by the calculated partition coefficient (P). The dashed ellipse-encircled symbols in Figure 4B plot the partition-corrected IC_{50} values for the four ligands considered in Figure 2 (and DIP-CH). The progressive loss of potency (DIP-PIC ~ DIP-P >> DIP-PT >>> DIP-PF) qualitatively tracks closer to the ability of the ligand to act as an H-bond acceptor (DIP-PIC > DIP-P > DIP-PT >>> DIP-PF) than a donor (DIP-P > DIP-PT >>> DIP-PIC ~ DIP-PF) with the most glaring potency-acceptor inconsistency being the behavior of isocyanate compared to hydroxyl. While isocyanate can theoretically accept 3 H-bonds but hydroxyl only one, DIP-PIC and DIP-P exhibit essentially identical potency. We posit that the similarity of DIP-PIC and DIP-

P is consistent with the 1-adduct acting as an H-bond acceptor in an environment where there is only a single H-bond donor available. Such a conclusion is inconsistent with ligand coupling to water and suggests the bond is a ligand-protein interaction.

3.3 Are the effects of alterations in position 1 chemistry energetically consistent with disruption of an H-bond?

Replacement of the 1-OH by F eliminates the capacity of this adduct to engage in H-bonding - either as a donor or an acceptor. Importantly, it does so with little effect on most other physicochemical properties of the molecule [43, 46]. Consequently, we can discretely ascribe alterations in the IC_{50} to disruption of H-bonding. Based on the data in Figures 3 and 4, we estimate that the shift in IC_{50} in response to replacing OH with F is between 46 to 1,870-fold as determined from the ratios of the observed IC_{50}s for DIP-P and DIP-PF (Figure 4A) and the partition-corrected IC_{50}s for those ligands (Figure 4B), respectively. These changes correspond to a 2.3 to 4.5 kCal mol^{-1} destabilization of association; energetically, the observed loss of potency is entirely consistent with the disruption of an H-bond.

3.4 Do differences in pKa influence the H-bonding profile of the phenyl and cyclohexanol derivatives?

As pKa's of the phenol and cyclohexanol derivatives are orders of magnitude larger than the experimental pH, the concentrations of ionized species will be very low. Differential presentation of the hydroxyls is unlikely to contribute to the observed behavior. While the pKa of sulphydryls is in the experimental range, as the site of action of the ligands appears to be in the largely anhydrous membranous space, differential ionization is unlikely to be a factor beyond influencing the partitioning coefficient – an effect already accounted for in the data in Tables 1 and 2 and Figure 4B.

3.5 Does the H-bond contribute to coupling energy?

At the highest concentrations, DIP-P (and DTB-P) elicit an ~ −40 mV shift in the $V_{1/2}$ of HCN1 gating. While we were unable to reach concentrations sufficient to obviously saturate the concentration response curves for DIP-PT, DIP-PIC or DIP-PF, the first two appear to trend towards an efficacy similar to that of DIP-P (and DTB-P). In contrast, the concentration response relation of DIP-PF appears to be flatter than the hydroxyl, thiol or isocyanate *iso*-propyl analogues, and it appears it may tend to a plateau less than −40 mV; this suggests the interaction energy at the 1-position does not absolutely partition towards initial binding but, rather, the 1-position contributes modestly to coupling energy.

3.6 The alkylbenzene site is large

To examine the role of ligand volume, we systematically and symmetrically varied the nature of the alkyl adducts on positions 2 and 6 and did so in the background of not only a hydroxyl on position 1 (top row) but also in the background of both a thiol (second row) and an isocyanate (third row).

Inspection of the hydroxyl-containing substituents appears to show a U-shaped dependence of potency on the alkyl identity (Figure 3). *Iso*-propyl and *tert*-butyl derivatives are

comparable with respect to potency but inclusion of either smaller (ethyl) or more extended (*sec*-butyl) side-chains results in a marked right-shift in the concentration-response curves. A plot of IC_{50} as a function of molecular volume supports this impression (Figure 4A). Although we do not have access to the complete alkyl adduct series for 1-position thiol or isocyanate families, these partial series exhibit a comparable trend to higher potency as the alkyl group tends towards the *iso*-propyl : *tert*-butyl apparent optimum (Figures 3, 4A).

These data suggest that there is a narrowly-defined pocket that alkylbenzene derivatives dock within. If the alkyl groups are too small the ligand does not orient correctly while if the groups get above a threshold, the ability of the ligands to enter the pocket is diminished. Such a conclusion would be consistent with the well described "cut-off" effect of anesthetics at other molecular targets [47–50] with the caveat that the changes considered here (increasing the number of carbons in the 2 and 6 alkyl adducts) increases not only ligand volume, they increase ligand hydrophobicity and, as such, increases the ligand's partition coefficient.

Figure 4B plots the partition-corrected IC_{50} values of the matrix of ligands as a function of their molecular volume. When we consider only those ligands where a clear inflection and rising phase is discernable in the concentration response relation (disregarding DM-P, DM-PIC, DM-CH, DE-CH, and DSB-CH) the dependence on volume below the apparent *iso*-propyl : *tert*-butyl optimum largely disappears.

There is one anomaly within this analysis. DM-PT exhibits a clear inverse agonist activity whereas DM-P and DM-PIC do not. Given that both hydroxyl and isocyanate are better H-bond acceptors than is a thiol, and hydroxyl a better donor (Table 1), this preference for thiol in the di-methyl family is unexpected. As DM-PT is more hydrophobic (logP 2.87) than either DM-P (logP 2.22) or DM-PIC (logP 1.49; Table 1), it is possible that the apparent discontinuity reflects an edge effect wherein DM-PT reaches an effective within-membrane concentration whereas what would otherwise be effective molecules (DM-P and DM-PIC) do not. However, this is unlikely to be the sole determinant. Thus, the observations that DE-PIC is effective despite a logP of 1.93 would argue against inadequate ligand partitioning into the membrane being the sole reason DM-P and DM-PIC are ineffective in comparison with DM-PT. The basis for the additional advantage afforded to DM-PT (or disadvantage of the hydroxyl and isocyanate dimethyl derivatives) is unclear.

What about the apparent suppression of effectiveness at alkyl sizes above that of *tert*-butyl? The response curve for DSB-P suggests it could be either a low potency and high efficacy full inverse agonist (the data in Figure 3 represent the foot of a curve that has a right-shifted IC_{50} of ~355 μM as shown by the thin green line) or a partial inverse agonist that has a higher potency and lower efficacy (the data in Figure 3 represent the maximal $V_{1/2}$ with an IC_{50} of ~30 μM). Given the low aqueous solubility of butyl phenols (~200 μM; [51]) we were unable to reliably address this question by simply increasing the range of the concentration response curve.

Importantly, as an IC_{50} of either 30 μM or 355 μM is markedly larger than that of DTB-P ($IC_{50} = 4.8$ μM) the upturn seen at larger volumes in Figure 4 is likely to be real. This

conclusion receives further support from the additivity/competition approach adopted below, that suggests DSB-P is indeed a low potency full inverse agonist. Together, these data are consistent with the notion that, while large (800 Å^3), the inverse agonist alkylphenol site has a defined volume and geometry.

3.7 Alkylbenzenes act *via* four, radially-arrayed, structurally-defined, sites

The observation that various congeners of DIP-P and DTB-P may exhibit partial inverse agonist behavior has important implications with respect to understanding the molecular interactions between this class of molecules and HCN1 and, hence, the development of a SAR profile for the presumptive inverse agonist site(s). Accordingly, we next examined whether the behavior of corresponding cyclohexanols and alkyl adduct-modified ligands could further inform us about the nature of the alkylbenzene:HCN1 channel interaction. Specifically, we sought to determine the answers to four fundamental questions: 1) Are the cyclohexanols and the short and long alkyl group phenols truly partial inverse agonists? 2) Does the behavior of cyclohexanols and phenols further validate the notion of a structurally-defined alkylbenzene site on HCN1 as opposed to a generalized perturbation effect? 3) Can the data inform us as to the stoichiometry and location of the presumptive alkylbenzene site(s)? 4) Can we elucidate the mechanistic basis for the loss of efficacy in the cyclohexanols?

The simplest ligand to consider is DE-P. The observed V$_{1/2}$ appears to a saturate at 100 μM. Indeed, in paired experiments we find the V$_{1/2}$ in the face of 100 and 300 μM to be indistinguishable (−21.6 mV ± 4.2, n = 8 and −21.2 mV ± 4.6, n = 9; respectively; P = 0.95, two-tailed t-test). Importantly, the aqueous solubility limit of DE-P (~10 mM; https://comptox.epa.gov/dashboard/dsstoxdb/results?search=DTXSID5061401#comments) is two-orders of magnitude higher than the functional saturation observed here. That is, DE-P is indeed a partial inverse agonist with a maximal efficacy ~2-fold lower than the maximal effect seen with DIP-P and DTB-P (see also Table 3). These data show the 2 and/or 6 adducts can "sense" changes in channel structure upon channel opening and, in this case, the effect of the smaller alkyl adduct is to reduce coupling energy.

With respect to the cyclohexanols, the maximal V$_{1/2}$ determined from fits of the Hill equation suggest there to be a >2-fold decrease in efficacy in the di-*iso*-propyl background and a >4-fold decrease in the *tert*-butyl background (Figure 3 and Table 3). This decrement is associated with little (*tert*-butyl) or only modest (*iso*-propyl) decrement in potency (see the green dashed lines in Figure 3). However, the low aqueous solubility of these cyclohexanols raises the concern that the apparent saturation of their concentration response curves is a function of ligand availability and not channel responsiveness. To address this, we presented HCN1 channels with a submaximal concentration of DTB-P in the absence and presence of increasing concentrations of DIP-CH and DTB-CH (as well as DIP-P, DSB-P and DE-CH) and considered the results within the context of the gating models outlined in Figure 1.

The symbols in Figure 5A–B reproduce the observed concentration response data (from Figure 3) for DIP-CH and DIP-P (Figure 5A) and DTB-CH and DTB-P (Figure 5B). Figure 5C–E present the shift in the V$_{1/2}$ elicited by increasing concentrations of DIP-CH (Figure

5C), DTB-CH (Figure 5D) and DIP-P (Figure 5E) in the presence of 3 μM DTB-P. The solid blue lines in Figure 5A–E represent the simultaneous fit of the common site model at S=4.

Qualitatively, the behaviors of DIP-CH and DTB-CH are exactly those expected for partial inverse agonists while DIP-P behaves exactly as expected for a second full inverse when all act at the same site(s) as DTB-P (Methods). Quantitatively, the optimized values of the ligand association constants are physically reasonable and the errors around each term are relatively modest (Table 4; Figure 5F). In contrast, the fit of the common site model at S=1 is inferior (χ^2 is 147 vs. 91 for S=4) and L adopts a physically unreasonable value of $7 * 10^8$ $\pm 5 * 10^8$.

We examined the reasonableness of the distinct-site models in two ways. First, we used the parameters reported in Table 4 and Figure 5F to predict the behavior of the distinct-site model at S=4. As anticipated (Methods) models of this class are, by definition, additive in the domain of inverse agonist concentrations where the $V_{1/2}$ is submaximal; the dashed blue lines in Figure 5C–E show poor or no correspondence to the observed data. Second, we fit the distinct-site model to the data. The fits were inferior to those of the single site model (χ^2 at S=4 was 263 and 809 at S=1). Furthermore, at both S=1 and S=4, one or more ligand association constants dropped to zero while, at S=1, L was unreasonably large and very poorly defined ($4.1 * 10^5 \pm 9.3 * 10^8$). It is important to note that as the distinct-site model is conceptually identical to a generalized membrane perturbation model, failure of the distinct model provides additional evidence for the existence of specific, structurally-defined, alkylbenzene site(s) on HCN1.

Consistent with the above findings, DE-CH exhibited neither additivity nor competition with 3 μM DTB-P (data not shown). While DE-CH appears to be only weakly effective as an inverse agonist (displaying an inflexion in the concentration response curve only at the highest concentration achieved - Figure 3) the lack of effect of DE-CH in the presence of DTB-P provides an additional control for potential non-specific effects of loading the cell membrane with these small molecules.

The simplest interpretation of these findings is that DTB-P (and DIP-P) act as full inverse agonists by interacting with four radially-arrayed binding sites lying within or between each HCN subunit, and that cyclohexanols (and ligands with altered alkyl adducts) associate with these same sites but generate less coupling energy than do the *iso*-propyl and *tert*-butyl phenols.

3.8 What is the basis for degradation of coupling energy upon conversion of a phenol to a cyclohexanol?

Figure 5F shows this arises from a preferential degradation in the association of the ligand with the closed state with a more modest disruption of open state affinity. In the background of *iso*-propyl and *tert*-butyl ligand families, the effect of ring saturation on closed and open state association is largely independent of the alkyl chain background (as shown by the comparable shifts in G - Figure 6F). This is consistent with these alkyl groups contributing comparably to channel-ligand association energies.

3.9   Extended alkyl chains disrupt ligand association with HCN1

Figure 6 shows the results of an additivity experiment directly comparable to that in Figure 5. While the achievable concentration range of DSB-P is a limiting factor and the fits are, consequently, poorly determined, the data are consistent with DSB-P being a low affinity full inverse agonist. As with the data for DIP-CH, DTB-CH and DIP-P, the behavior of DSB-P was best described by the common-site model S=4.

4.   Discussion

Four key chemical characteristics define congeners of DIP-P - H-bond propensity, ring saturation/planarity, hydrophobicity, and molecular volume. We find that: 1) There is an alkylbenzene site on HCN1 channels that is relatively large, having a volume   800 Å^3; 2) The site contains an H-bond donor that interacts with the 1-position adduct on the ligand in a manner that contributes to initial binding energy; 3) The 1-position adduct is, at best, poorly involved with generation of coupling energy indicating the site's hydrogen bond donor is relatively immobile (with respect to ligand) during channel opening; 4) The presence of a π electron cloud is coupled to the generation of coupling energy suggesting that these electrons (or the imposed ring planarity) is important in establishing a preferential association between the ligands and the closed state(s) of the channel; 5) Substituents at the 2 and 6 positions of the ligand (and possibly others excluding the 1-position) interact with aspects of the channel that are structurally dynamic during opening; 6) The data are most readily reconciled with the existence of four radially-arrayed alkylbenzene sites suggesting the sites lie within each HCN1 subunit or at the inter-subunit interface and these sites are distant (in terms of ligand geometry) from the central axis of the channel; 7) Addition of adducts capable of forming more specific interactions than permitted by alkyl chemistry may better exploit the state dependent channel surface and generate a higher potency class of inverse agonists.

4.1   Reasonableness of the common site, S=4, gating parameters

The best test of a model is to have it predict data not included in the fit. While we cannot readily gain independent measures of the association constants, we can independently estimate L. Based on the maximal open probability (P_{MAX}) we estimate L to be between 7.3 and 679 (Methods). That our model-determined measure of L (125) falls within this range suggests the model determined parameters are consistent with the energetics of HCN1 gating and drug effects thereon.

Does our use of a simple three-state gating scheme undermine the validity of this analysis? While the model shown in Figure 1 does not reproduce the nuanced kinetic behavior of HCN channels ([37] and references therein), the general form of the relationships between L, P_{MAX} and $V_{1/2}$ in more complex, kinetically-faithful, models will be comparable to equations 7 and 8 (albeit such solutions will contain proportionality terms based on the presence of additional coupled equilibria). Any quantitative impact on the estimates of L from such an increase in the complexity of the basal gating model will equivalently impact its determination from the additivity data in Figure 5 and the NSFA studies. Accordingly, we posit that the analysis of inverse agonists and partial inverse agonists predicts a

physiologically-reasonable determination of the fully-activated open-closed equilibrium which will remain true with any such model expansion.

4.2   How does ring planarity and/or the π electron cloud contribute to coupling energy?

What is the likely basis for the preferential loss of closed state binding upon ring saturation? One possibility is that the π electrons form an electrostatic bond with the channel that is stronger in the closed state than in the open state. The ~1 kCal mol^{-1} degradation in Kc on shifting from the phenolic structure to the cyclohexanol is energetically consistent with such a scenario [52]. An alternative scenario is that the rigid structure of the phenolic ring acts as a better "foot-in-the-door" than does the more flexible cyclohexanol. Distinguishing between these mechanisms could be aided by use of fluorine for ring-hydrogen substitution analogues [53, 54] in the background of either DIP-P or DTB-P, but those studies are beyond the scope of the current manuscript.

4.3   Do the chemical characteristics identified here correspond to known alkylbenzene binding sites?

The existence of spatially-defined cavities (*i.e.*, presumptive functional binding sites) that can accommodate small anesthetic molecules have been identified in a variety of proteins, including firefly luciferase, human serum albumin, and both ligand- and voltage-gated ion channels [55–57]. Modeling based on molecular mechanics–quantum mechanics calculations suggest that anesthetic-protein complexes share a set of common characteristics, or "binding motifs"; these motifs are "polar and nonpolar interactions within an amphiphilic binding cavity, including the presence of weak hydrogen bond interactions with amino acids and water molecules" [58]. The results presented herein suggest the existence of a spatially-defined cavity in HCN1 channels that accommodates small lipophilic molecules and that the underlying interactions conform to the previously proposed "binding motifs."

4.4   Mapping the isoform divergence onto the HCN1 cryo-EM structure

HCN1 is the isoform most sensitive to alkylphenols with HCN2, 3 and 4 being progressively less sensitive albeit with some dependence on the alkyl side chain identity (*iso-propyl* versus *tert-butyl*) [22]. With respect to trying to identify key residues that determine the potency and efficacy of alkylphenol inhibition, this profile suggests residues that are unique to HCN1 may not be the complete picture but that locations that follow a divergence in conservation may also be important.

Figure 7 shows within the transmembrane structure of HCN1- Nv C, the minimal HCN1 channel that retains alkylphenol sensitivity, there are residues unique to HCN1 and others divergent between the four isoforms. While our hypothesis is that residues contacting, or within, the S5-S6 motif are most likely to contribute to the site, it is clear that there are too many divergent locations to justify a site-directed analysis (with all its inherent caveats of interpretation). Accordingly, identification of the alkylbenzene sites will likely be best determined using photolabeling and chimeric approaches combined with molecular docking strategies once the open and closed architectures of the HCN1 channel are known [55]. The results presented here will allow for rationale interpretation of the findings of any, and all, such studies.

4.5 Alkylphenols as novel antihyperalgesics and addiction potential

Might propofol, and by extension other alkylphenols, interact with other signaling pathways, especially those centered on the opiate receptor system? *In vitro*, propofol has no direct effect on G-protein coupled inwardly rectifying K$^+$ channels (GIRKs), nor does a clinically relevant concentration of propofol (2 μM) potentiate D-Ala^2,*N*-Me-Phe^4,Gly^5-ol]enkephalin (DAMGO)-evoked currents generated by GIRK2 channels [59]; importantly, and in contrast, supratherapeutic propofol concentrations (up to 100 μM propofol, a 50×-clinically relevant concentration) inhibit DAMGO-evoked currents generated by chimeric mu opiate (μOR-G$_{qi5}$) receptors [60]. Thus, there is no evidence that propofol potentiates mu opiate receptor (mOR) function at the molecular level [61]. As to other alkylphenols, DTB-P, like propofol, inhibits HCN1 gating [22], but unlike propofol, it has minimal activity at GABA$_A$ receptors [42] although it increases open channel probability (P$_o$) of α3β glycine receptors [23]; there are no published data on the effects of DTB-P on G-protein coupled receptors in general, and mORs in particular. Despite increasing P$_o$ of α3β glycine receptors, α3β glycine receptors do not contribute to either DTB-P-mediated mechanical or thermal anti-hyperalgesia following chronic constriction nerve injury [23], an effect comparable to our observations using a partial sciatic nerve ligation model of neuropathic pain [22].

With regards to analgesia and modulation of pain pathways *in vivo*, propofol suppresses activity of spinal cord dorsal horn neurons in response to noxious stimulation in goats [62] and rats [63], and this effect appears to be partly GABAergic in origin [63]. In human subjects, however, a meta-analysis of thirty-nine clinical trials with a combined subject population of 4,520 patients indicated that propofol-based anesthetics do not result in less postoperative pain than those utilizing volatile anesthetics [64], suggesting that propofol *per se* does not produce meaningful analgesia that extends into the immediate postoperative period. Such an observation does not preclude the development of alkylphenols as anti-hyperalgesics as anti-hyperalgesia is not the same as analgesia, reflecting the fact that *pain* - "an unpleasant sensory and emotional experience associated with actual or potential tissue damage" is not equivalent to *hyperalgesia* – "increased pain from a stimulus that normally provokes pain" (https://www.iasp-pain.org/terminology?navItemNumber=576). The *in vivo* data comport with the *in vitro* data and suggest that propofol, and presumably related alkylphenols, should have a good therapeutic index with respect to the risk of addiction as the relevant circuitry underlying opioid-dependent addiction [65, 66] and propofol mechanisms of action [67, 68] do not overlap.

Our data suggest that a spatially defined cavity that accommodates alkylphenols exists in the transmembrane or interfacial region of HCN1. Whether the binding site is similar to comparable binding sites in other channels, including GABA$_A$ [26, 69], TRPA1 [70, 71], and glycine [23], receptors remains to be determined. Given the size of the pocket and the lack of specific chemical interactions with alkyl adducts, the findings suggest it may be possible to develop a higher potency analogue of DTB-P with drug-like properties, particularly as the HCN1 cryo-EM structure is now available [33]. Such experiments have the potential to reveal a new, opioid-independent approach to treating neuropathic pain.

Acknowledgements

Abbreviations:

GABA$_A$-Rs	GABA$_A$ receptors
HCN	hyperpolarization cyclic nucleotide gated channel
NSFA	non-stationary fluctuation analysis
P$_{MAX}$	maximal open probability
SAR	structure-activity relationship
TEVC	two-electrode voltage clamp
DM-P	2,6-di-methyl phenol
DM-PT	2,6 di-methyl phenyl-thiol
DM-PIC	2,6-di-methyl phenyl-isocyanate
DM-PF	2,6-di-methyl phenyl-fluorine
DM-CH	2,6-di-methyl cyclohexanol
DE-P	2,6-di-ethyl phenol
DE-PT	2,6 di-ethyl phenyl-thiol
DE-PIC	2,6 di-ethyl phenyl-isocyanate
DE-PF	2,6-di-ethyl phenyl-flurorine
DE-CH	2,6 di-ethyl cyclohexanol
DIP-P	2,6 di-*iso*-propyl phenol (propofol)
DIP-PT	2,6-di-*iso*-propyl phenyl-thiol
DIP-PIC	2,6-di-*iso*-propyl phenyl-isocyanate
DIP-PF	2,6-di-*iso*-propyl phenyl-fluorine
DIP-CH	2,6 di-*iso*-propyl cyclohexanol
DSB-P	2,6-di-*sec*-butyl phenol
DSB-PT	2,6-di-*sec*-butyl phenyl-thiol

DSB-PIC	2,6 di-*sec*-butyl phenyl-isocyanate
DSB-PF	2,6-di-*sec*-butyl phenyl-fluorine
DSB-CH	2,6 di-*sec*-butyl cyclohexanol
DTB-P	2,6-di-*tert*-butyl phenol
DTB-PT	2,6-di-*tert*-butyl phenyl-thiol
DTB-PIC	2,6 di-*tert*-butyl phenyl-isocyanate
DTB-PF	2,6 di-*tert*-butyl phenyl-fluorine
DTB-CH	2,6 di-*tert*-butyl cycloxhexanol

References

[1]. Costigan M, Scholz J, Woolf CJ, Neuropathic pain: a maladaptive response of the nervous system to damage, Annu Rev Neurosci 32 (2009) 1–32. 10.1146/annurev.neuro.051508.135531. [PubMed: 19400724]

[2]. Colloca L, Ludman T, Bouhassira D, Baron R, Dickenson AH, Yarnitsky D, Freeman R, Truini A, Attal N, Finnerup NB, Eccleston C, Kalso E, Bennett DL, Dworkin RH, Raja SN, Neuropathic pain, Nat Rev Dis Primers 3 (2017) 17002 10.1038/nrdp.2017.2. [PubMed: 28205574]

[3]. Freynhagen R, Bennett MI, Diagnosis and management of neuropathic pain, BMJ 339 (2009) b3002 10.1136/bmj.b3002. [PubMed: 19675082]

[4]. Seretny M, Currie GL, Sena ES, Ramnarine S, Grant R, MacLeod MR, Colvin LA, Fallon M, Incidence, prevalence, and predictors of chemotherapy-induced peripheral neuropathy: A systematic review and meta-analysis, Pain 155(12) (2014) 2461–70. 10.1016/j.pain.2014.09.020. [PubMed: 25261162]

[5]. Bouhassira D, Lanteri-Minet M, Attal N, Laurent B, Touboul C, Prevalence of chronic pain with neuropathic characteristics in the general population, Pain 136(3) (2008) 380–7. 10.1016/j.pain.2007.08.013. [PubMed: 17888574]

[6]. van Hecke O, Austin SK, Khan RA, Smith BH, Torrance N, Neuropathic pain in the general population: a systematic review of epidemiological studies, Pain 155(4) (2014) 654–62. 10.1016/j.pain.2013.11.013. [PubMed: 24291734]

[7]. Finnerup NB, Attal N, Haroutounian S, McNicol E, Baron R, Dworkin RH, Gilron I, Haanpaa M, Hansson P, Jensen TS, Kamerman PR, Lund K, Moore A, Raja SN, Rice AS, Rowbotham M, Sena E, Siddall P, Smith BH, Wallace M, Pharmacotherapy for neuropathic pain in adults: a systematic review and meta-analysis, Lancet Neurol 14(2) (2015) 162–73. 10.1016/S1474-4422(14)70251-0. [PubMed: 25575710]

[8]. Baron R, Maier C, Attal N, Binder A, Bouhassira D, Cruccu G, Finnerup NB, Haanpää M, Hansson P, Hüllemann P, Jensen TS, Freynhagen R, Kennedy JD, Magerl W, Mainka T, Reimer M, Rice AS, Segerdahl M, Serra J, Sindrup S, Sommer C, Tölle T, Vollert J, Treede RD, Peripheral neuropathic pain: a mechanism-related organizing principle based on sensory profiles, Pain 158(2) (2017) 261–272. 10.1097/j.pain.0000000000000753. [PubMed: 27893485]

[9]. West SJ, Bannister K, Dickenson AH, Bennett DL, Circuitry and plasticity of the dorsal horn-- toward a better understanding of neuropathic pain, Neuroscience 300 (2015) 254–75. 10.1016/j.neuroscience.2015.05.020. [PubMed: 25987204]

[10]. Tibbs GR, Posson DJ, Goldstein PA, Voltage-Gated Ion Channels in the PNS: Novel Therapies for Neuropathic Pain?, Trends Pharmacol Sci 37(7) (2016) 522–42. 10.1016/j.tips.2016.05.002. [PubMed: 27233519]

[11]. Chaplan SR, Guo HQ, Lee DH, Luo L, Liu C, Kuei C, Velumian AA, Butler MP, Brown SM, Dubin AE, Neuronal hyperpolarization-activated pacemaker channels drive neuropathic pain, J Neurosci 23(4) (2003) 1169–78. 10.1523/JNEUROSCI.23-04-01169.2003. [PubMed: 12598605]

[12]. Luo L, Chang L, Brown SM, Ao H, Lee DH, Higuera ES, Dubin AE, Chaplan SR, Role of peripheral hyperpolarization-activated cyclic nucleotide-modulated channel pacemaker channels in acute and chronic pain models in the rat, Neuroscience 144(4) (2007) 1477–85. 10.1016/j.neuroscience.2006.10.048. [PubMed: 17196750]

[13]. Jiang YQ, Xing GG, Wang SL, Tu HY, Chi YN, Li J, Liu FY, Han JS, Wan Y, Axonal accumulation of hyperpolarization-activated cyclic nucleotide-gated cation channels contributes to mechanical allodynia after peripheral nerve injury in rat, Pain 137(3) (2008) 495–506. 10.1016/j.pain.2007.10.011. [PubMed: 18179873]

[14]. Takasu K, Ono H, Tanabe M, Spinal hyperpolarization-activated cyclic nucleotide-gated cation channels at primary afferent terminals contribute to chronic pain, Pain 151(1) (2010) 87–96. 10.1016/j.pain.2010.06.020. [PubMed: 20619969]

[15]. Noh S, Kumar N, Bukhanova N, Chen Y, Stemkowsi PL, Smith PA, The heart-rate-reducing agent, ivabradine, reduces mechanical allodynia in a rodent model of neuropathic pain, Eur J Pain 18(8) (2014) 1139–47. 10.1002/j.1532-2149.2014.00460.x. [PubMed: 24677354]

[16]. Young GT, Emery EC, Mooney ER, Tsantoulas C, McNaughton PA, Inflammatory and neuropathic pain are rapidly suppressed by peripheral block of hyperpolarisation-activated cyclic nucleotide-gated ion channels, Pain 155(9) (2014) 1708–19. 10.1016/j.pain.2014.05.021. [PubMed: 24861581]

[17]. Descoeur J, Pereira V, Pizzoccaro A, Francois A, Ling B, Maffre V, Couette B, Busserolles J, Courteix C, Noel J, Lazdunski M, Eschalier A, Authier N, Bourinet E, Oxaliplatin-induced cold hypersensitivity is due to remodelling of ion channel expression in nociceptors, EMBO molecular medicine 3(5) (2011) 266–78. 10.1002/emmm.201100134. [PubMed: 21438154]

[18]. Zhang H, Dougherty PM, Enhanced excitability of primary sensory neurons and altered gene expression of neuronal ion channels in dorsal root ganglion in paclitaxel-induced peripheral neuropathy, Anesthesiology 120(6) (2014) 1463–75. 10.1097/ALN.0000000000000176. [PubMed: 24534904]

[19]. Aromolaran KA, Goldstein PA, [EXPRESS] Ion channels and neuronal hyperexcitability in chemotherapy-induced peripheral neuropathy; cause and effect?, Mol Pain 13 (2017) 1744806917714693 10.1177/1744806917714693. [PubMed: 28580836]

[20]. Tu H, Zhang L, Tran TP, Muelleman RL, Li YL, Diabetes alters protein expression of hyperpolarization-activated cyclic nucleotide-gated channel subunits in rat nodose ganglion cells, Neuroscience 165(1) (2010) 39–52. 10.1016/j.neuroscience.2009.10.002. [PubMed: 19815055]

[21]. McClure KJ, Maher M, Wu N, Chaplan SR, Eckert WA III, Lee DH, Wickenden AD, Hermann M, Allison B, Hawryluk N, Breitenbucher JG, Grice CA, Discovery of a novel series of selective HCN1 blockers, Bioorg Med Chem Lett 21(18) (2011) 5197–201. 10.1016/j.bmcl.2011.07.051. [PubMed: 21824780]

[22]. Tibbs GR, Rowley TR, Sanford RL, Herold KF, Proekt A, Hemmings HC, Andersen OS, Goldstein PA, Flood P, HCN1 channels as targets for anesthetic and non-anesthetic propofol analogs in the amelioration of mechanical and thermal hyperalgesia in a mouse model of neuropathic pain, J Pharmacol Exp Ther 345 (2013) 363–373. 10.1124/jpet.113.203620. [PubMed: 23549867]

[23]. Acuña MA, Yévenes GE, Ralvenius WT, Benke D, Di Lio A, Lara CO, Muñoz B, Burgos CF, Moraga-Cid G, Corringer PJ, Zeilhofer HU, Phosphorylation state-dependent modulation of spinal glycine receptors alleviates inflammatory pain, J Clin Invest 126(7) (2016) 2547–60. 10.1172/JCI83817. [PubMed: 27270175]

[24]. Resta F, Micheli L, Laurino A, Spinelli V, Mello T, Sartiani L, Di Cesare Mannelli L, Cerbai E, Ghelardini C, Romanelli MN, Mannaioni G, Masi A, Selective HCN1 block as a strategy to control oxaliplatin-induced neuropathy, Neuropharmacology 131 (2018) 403–413. 10.1016/j.neuropharm.2018.01.014. [PubMed: 29339292]

[25]. Lyashchenko AK, Redd KJ, Yang J, Tibbs GR, Propofol inhibits HCN1 pacemaker channels by selective association with the closed states of the membrane embedded channel core, J Physiol 583(Pt 1) (2007) 37–56. 10.1113/jphysiol.2007.136465. [PubMed: 17569731]

[26]. Jayakar SS, Zhou X, Chiara DC, Dostalova Z, Savechenkov PY, Bruzik KS, Dailey WP, Miller KW, Eckenhoff RG, Cohen JB, Multiple propofol-binding sites in a γ-aminobutyric acid type A

receptor (GABAAR) identified using a photoreactive propofol analog, J Biol Chem 289(40) (2014) 27456–68. 10.1074/jbc.M114.581728. [PubMed: 25086038]

[27]. Forman SA, Miller KW, Mapping General Anesthetic Sites in Heteromeric γ-Aminobutyric Acid Type A Receptors Reveals a Potential For Targeting Receptor Subtypes, Anesth Analg 123(5) (2016) 1263–1273. 10.1213/ANE.0000000000001368. [PubMed: 27167687]

[28]. Nury H, Van Renterghem C, Weng Y, Tran A, Baaden M, Dufresne V, Changeux JP, Sonner JM, Delarue M, Corringer PJ, X-ray structures of general anaesthetics bound to a pentameric ligand-gated ion channel, Nature 469(7330) (2011) 428–31. 10.1038/nature09647. [PubMed: 21248852]

[29]. Franks NP, General anaesthesia: from molecular targets to neuronal pathways of sleep and arousal, Nat Rev Neurosci 9(5) (2008) 370–86. 10.1038/nrn2372. [PubMed: 18425091]

[30]. Hemmings HC Jr., Akabas MH, Goldstein PA, Trudell JR, Orser BA, Harrison NL, Emerging molecular mechanisms of general anesthetic action, Trends Pharmacol Sci 26(10) (2005) 503–10. 10.1016/j.tips.2005.08.006. [PubMed: 16126282]

[31]. Brosnan RJ, Pham TL, GABA$_A$ Receptor Modulation by Phenyl Ring Compounds Is Associated with a Water Solubility Cut-Off Value, Pharmacology 98(1–2) (2016) 13–9. 10.1159/000444935. [PubMed: 26986632]

[32]. Long SB, Tao X, Campbell EB, MacKinnon R, Atomic structure of a voltage-dependent K$^+$ channel in a lipid membrane-like environment, Nature 450(7168) (2007) 376–82. 10.1038/nature06265. [PubMed: 18004376]

[33]. Lee CH, MacKinnon R, Structures of the Human HCN1 Hyperpolarization-Activated Channel, Cell 168(1–2) (2017) 111–120 e11. 10.1016/j.cell.2016.12.023. [PubMed: 28086084]

[34]. Riegelhaupt PM, Tibbs GR, Goldstein PA, HCN and K$_{2P}$ Channels in Anesthetic Mechanisms Research, Methods Enzymol 602 (2018) 391–416. 10.1016/bs.mie.2018.01.015. [PubMed: 29588040]

[35]. Bezanilla F, Stefani E, Voltage-dependent gating of ionic channels, Annu Rev Biophys Biomol Struct 23 (1994) 819–46. 10.1146/annurev.bb.23.060194.004131. [PubMed: 7522668]

[36]. Bezanilla F, The voltage sensor in voltage-dependent ion channels, Physiol Rev 80(2) (2000) 555–92. 10.1152/physrev.2000.80.2.555. [PubMed: 10747201]

[37]. Lyashchenko AK, Redd KJ, Goldstein PA, Tibbs GR, cAMP Control of HCN2 Channel Mg^{2+} Block Reveals Loose Coupling between the Cyclic Nucleotide-Gating Ring and the Pore, PLoS One 9(7) (2014) e101236 10.1371/journal.pone.0101236. [PubMed: 24983358]

[38]. Azene EM, Xue T, Li RA, Molecular basis of the effect of potassium on heterologously expressed pacemaker (HCN) channels, J Physiol 547(Pt 2) (2003) 349–56. 10.1113/jphysiol.2003.039768. [PubMed: 12562911]

[39]. Shin KS, Maertens C, Proenza C, Rothberg BS, Yellen G, Inactivation in HCN channels results from reclosure of the activation gate: desensitization to voltage, Neuron 41(5) (2004) 737–44. 10.1016/S0896-6273(04)00083-2. [PubMed: 15003173]

[40]. Craven KB, Zagotta WN, Salt bridges and gating in the COOH-terminal region of HCN2 and CNGA1 channels, J Gen Physiol 124(6) (2004) 663–77. 10.1085/jgp.200409178. [PubMed: 15572346]

[41]. Chen S, Wang J, Zhou L, George MS, Siegelbaum SA, Voltage sensor movement and cAMP binding allosterically regulate an inherently voltage-independent closed-open transition in HCN channels, J Gen Physiol 129(2) (2007) 175–88. 10.1085/jgp.200609585. [PubMed: 17261842]

[42]. Krasowski MD, Jenkins A, Flood P, Kung AY, Hopfinger AJ, Harrison NL, General anesthetic potencies of a series of propofol analogs correlate with potency for potentiation of γ-aminobutyric acid (GABA) current at the GABA$_A$ receptor but not with lipid solubility, J Pharmacol Exp Ther 297(1) (2001) 338–51. [PubMed: 11259561]

[43]. Woll KA, Weiser BP, Liang Q, Meng T, McKinstry-Wu A, Pinch B, Dailey WP, Gao WD, Covarrubias M, Eckenhoff RG, Role for the Propofol Hydroxyl in Anesthetic Protein Target Molecular Recognition, ACS Chem Neurosci 6(6) (2015) 927–35. 10.1021/acschemneuro.5b00078. [PubMed: 25799399]

[44]. Denmark SE, Hartmann E, Kornfilt DJ, Wang H, Mechanistic, crystallographic, and computational studies on the catalytic, enantioselective sulfenofunctionalization of alkenes, Nat Chem 6(12) (2014) 1056–64. 10.1038/nchem.2109. [PubMed: 25411883]

[45]. Hall AC, Griffith TN, Tsikolia M, Kotey FO, Gill N, Humbert DJ, Watt EE, Yermolina YA, Goel S, El-Ghendy B, Hall CD, Cyclohexanol analogues are positive modulators of GABA_A receptor currents and act as general anaesthetics in vivo, Eur J Pharmacol 667(1–3) (2011) 175–81. 10.1016/j.ejphar.2011.05.058. [PubMed: 21658385]

[46]. Qiu L, Lin J, Liu Q, Wang S, Lv G, Li K, Shi H, Huang Z, Bertaccini EJ, The Role of the Hydroxyl Group in Propofol-Protein Target Recognition: Insights from ONIOM Studies, J Phys Chem B 121(24) (2017) 5883–5896. 10.1021/acs.jpcb.7b02079. [PubMed: 28548837]

[47]. Jenkins A, Greenblatt EP, Faulkner HJ, Bertaccini E, Light A, Lin A, Andreasen A, Viner A, Trudell JR, Harrison NL, Evidence for a common binding cavity for three general anesthetics within the GABA_A receptor, J Neurosci 21(6) (2001) RC136 10.1523/JNEUROSCI.21-06-j0002.2001. [PubMed: 11245705]

[48]. Krasowski MD, Nishikawa K, Nikolaeva N, Lin A, Harrison NL, Methionine 286 in transmembrane domain 3 of the GABA_A receptor β subunit controls a binding cavity for propofol and other alkylphenol general anesthetics, Neuropharmacology 41(8) (2001) 952–64. [PubMed: 11747900]

[49]. Krasowski MD, Hong X, Hopfinger AJ, Harrison NL, 4D-QSAR analysis of a set of propofol analogues: mapping binding sites for an anesthetic phenol on the GABA_A receptor, J Med Chem 45(15) (2002) 3210–21. 10.1021/jm010461a. [PubMed: 12109905]

[50]. Kash TL, Jenkins A, Harrison NL, Molecular volume determines the activity of the halogenated alkane bromoform at wild-type and mutant GABA(A) receptors, Brain Res 960(1–2) (2003) 36–41. 10.1016/S0006-8993(02)03748-4. [PubMed: 12505655]

[51]. Brewster ME, Braunstein AJ, Bartruff MSM, Kibbey C, Huang M-J, Pop E, Bodor N, Solubilization and electrochemical stabilization of substituted phenols through the use of 2-hydroxypropyl-β-cyclodextrin, Supramolecular Chemistry 4(1) (1994) 69–76. DOI: 10.1080/10610279408029864.

[52]. Neel AJ, Hilton MJ, Sigman MS, Toste FD, Exploiting non-covalent π interactions for catalyst design, Nature 543(7647) (2017) 637–646. 10.1038/nature21701. [PubMed: 28358089]

[53]. Ahern CA, Eastwood AL, Lester HA, Dougherty DA, Horn R, A cation-π interaction between extracellular TEA and an aromatic residue in potassium channels, J Gen Physiol 128(6) (2006) 649–57. 10.1085/jgp.200609654. [PubMed: 17130518]

[54]. Van Arnam EB, Dougherty DA, Functional probes of drug-receptor interactions implicated by structural studies: Cys-loop receptors provide a fertile testing ground, J Med Chem 57(15) (2014) 6289–300. 10.1021/jm500023m. [PubMed: 24568098]

[55]. Franks NP, Structural comparisons of ligand-gated ion channels in open, closed, and desensitized states identify a novel propofol-binding site on mammalian gamma-aminobutyric acid type A receptors, Anesthesiology 122(4) (2015) 787–94. 10.1097/ALN.0000000000000588. [PubMed: 25575161]

[56]. Chen Q, Xu Y, Tang P, X-Ray Crystallographic Studies for Revealing Binding Sites of General Anesthetics in Pentameric Ligand-Gated Ion Channels, Methods Enzymol 603 (2018) 21–47. 10.1016/bs.mie.2018.01.017. [PubMed: 29673527]

[57]. Bu W, Liang Q, Zhi L, Maciunas L, Loll PJ, Eckenhoff RG, Covarrubias M, Sites and Functional Consequence of Alkylphenol Anesthetic Binding to Kv1.2 Channels, Mol Neurobiol 55(2) (2018) 1692–1702. 10.1007/s12035-017-0437-2. [PubMed: 28204960]

[58]. Bertaccini EJ, Trudell JR, Franks NP, The common chemical motifs within anesthetic binding sites, Anesth Analg 104(2) (2007) 318–24. 10.1213/01.ane.0000253029.67331.8d. [PubMed: 17242087]

[59]. Yamakura T, Lewohl JM, Harris RA, Differential effects of general anesthetics on G protein-coupled inwardly rectifying and other potassium channels, Anesthesiology 95(1) (2001) 144–53. [PubMed: 11465552]

[60]. Minami K, Sudo Y, Shiraishi S, Seo M, Uezono Y, Analysis of the effects of anesthetics and ethanol on μ-opioid receptor, Journal of pharmacological sciences 112(4) (2010) 424–31. 10.1254/jphs.10003FP. [PubMed: 20379080]

[61]. Minami K, Uezono Y, The recent progress in research on effects of anesthetics and analgesics on G protein-coupled receptors, J Anesth 27(2) (2013) 284–92. 10.1007/s00540-012-1507-2. [PubMed: 23099434]

[62]. Antognini JF, Wang XW, Piercy M, Carstens E, Propofol directly depresses lumbar dorsal horn neuronal responses to noxious stimulation in goats, Can J Anaesth 47(3) (2000) 273–9. 10.1007/BF03018926. [PubMed: 10730741]

[63]. Takazawa T, Furue H, Nishikawa K, Uta D, Takeshima K, Goto F, Yoshimura M, Actions of propofol on substantia gelatinosa neurones in rat spinal cord revealed by *in vitro* and *in vivo* patch-clamp recordings, Eur J Neurosci 29(3) (2009) 518–28. 10.1111/j.1460-9568.2008.06607.x. [PubMed: 19222560]

[64]. Peng K, Liu HY, Wu SR, Liu H, Zhang ZC, Ji FH, Does Propofol Anesthesia Lead to Less Postoperative Pain Compared With Inhalational Anesthesia?: A Systematic Review and Meta-analysis, Anesth Analg 123(4) (2016) 846–58. 10.1213/ANE.0000000000001504. [PubMed: 27636574]

[65]. Rosen LG, Sun N, Rushlow W, Laviolette SR, Molecular and neuronal plasticity mechanisms in the amygdala-prefrontal cortical circuit: implications for opiate addiction memory formation, Frontiers in neuroscience 9 (2015) 399 10.3389/fnins.2015.00399. [PubMed: 26594137]

[66]. Langlois LD, Nugent FS, Opiates and Plasticity in the Ventral Tegmental Area, ACS Chem Neurosci 8(9) (2017) 1830–1838. 10.1021/acschemneuro.7b00281. [PubMed: 28768409]

[67]. Zhang H, Wang W, Zhao Z, Ge Y, Zhang J, Yu D, Chai W, Wu S, Xu L, The action sites of propofol in the normal human brain revealed by functional magnetic resonance imaging, Anat Rec (Hoboken) 293(12) (2010) 1985–90. 10.1002/ar.21069. [PubMed: 21207521]

[68]. Song XX, Yu BW, Anesthetic effects of propofol in the healthy human brain: functional imaging evidence, J Anesth 29(2) (2015) 279–88. 10.1007/s00540-014-1889-4. [PubMed: 25056258]

[69]. Woll KA, Murlidaran S, Pinch BJ, Henin J, Wang X, Salari R, Covarrubias M, Dailey WP, Brannigan G, Garcia BA, Eckenhoff RG, A Novel Bifunctional Alkylphenol Anesthetic Allows Characterization of GABA$_A$ Receptor Subunit Binding Selectivity in Synaptosomes, J Biol Chem 291(31) (2016) 20473–20486. 10.1074/jbc.M116.736975. [PubMed: 27462076]

[70]. Ton HT, Phan TX, Abramyan AM, Shi L, Ahern GP, Identification of a putative binding site critical for general anesthetic activation of TRPA1, Proc Natl Acad Sci U S A 114(14) (2017) 3762–3767. 10.1073/pnas.1618144114. [PubMed: 28320952]

[71]. Woll KA, Skinner KA, Gianti E, Bhanu NV, Garcia BA, Carnevale V, Eckenhoff RG, Gaudet R, Sites Contributing to TRPA1 Activation by the Anesthetic Propofol Identified by Photoaffinity Labeling, Biophys J 113 (2017) 1–5. 10.1016/j.bpj.2017.08.040. [PubMed: 28700907]
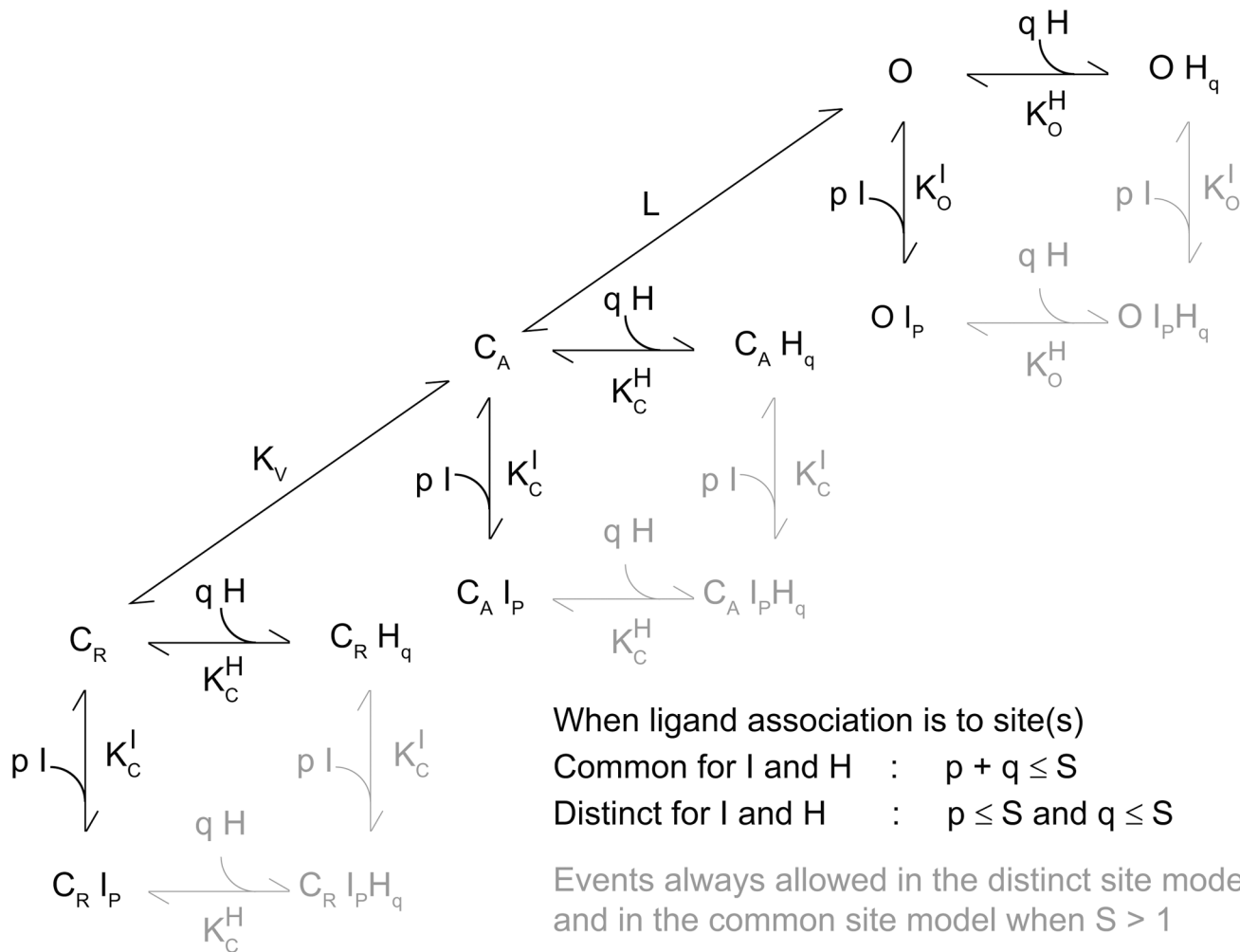
Figure 1: Alkylphenol and alkylcyclohexanol interaction with HCN1 channel gating modeled as, respectively, inverse agonist and partial inverse agonist coupling to channel opening.

C_R, C_A and O represent the closed-resting, closed-activated and open states; K_V and L the equilibrium constants describing activation and opening; I and H are an inverse agonist and a partial inverse agonist; p and q represent the number of binding events of I and H; K_C and K_O represent the association constants for I and H to closed and open channels with reference to I and H denoted by the appropriate superscript. For simplicity, only activation and opening transitions between un-liganded states are shown but all C_R-C_A and C_A-O transitions are permissible. When H and I associate with common site(s) the model contains 3 states *per* plane, 9 states in total (S=1) and 15 states per plane, 45 states in total (S=4). When H and I associate with distinct site(s) the model contains 4 states *per* plane, 12 states in total (S=1) and 25 states per plane, 75 states in total (S=4). Importantly, as the equilibrium constants are the only free parameters and the number of equilibrium constants is independent of the expansion of the number of states, each of these models should be equally well determined if they are equally able to describe the data.
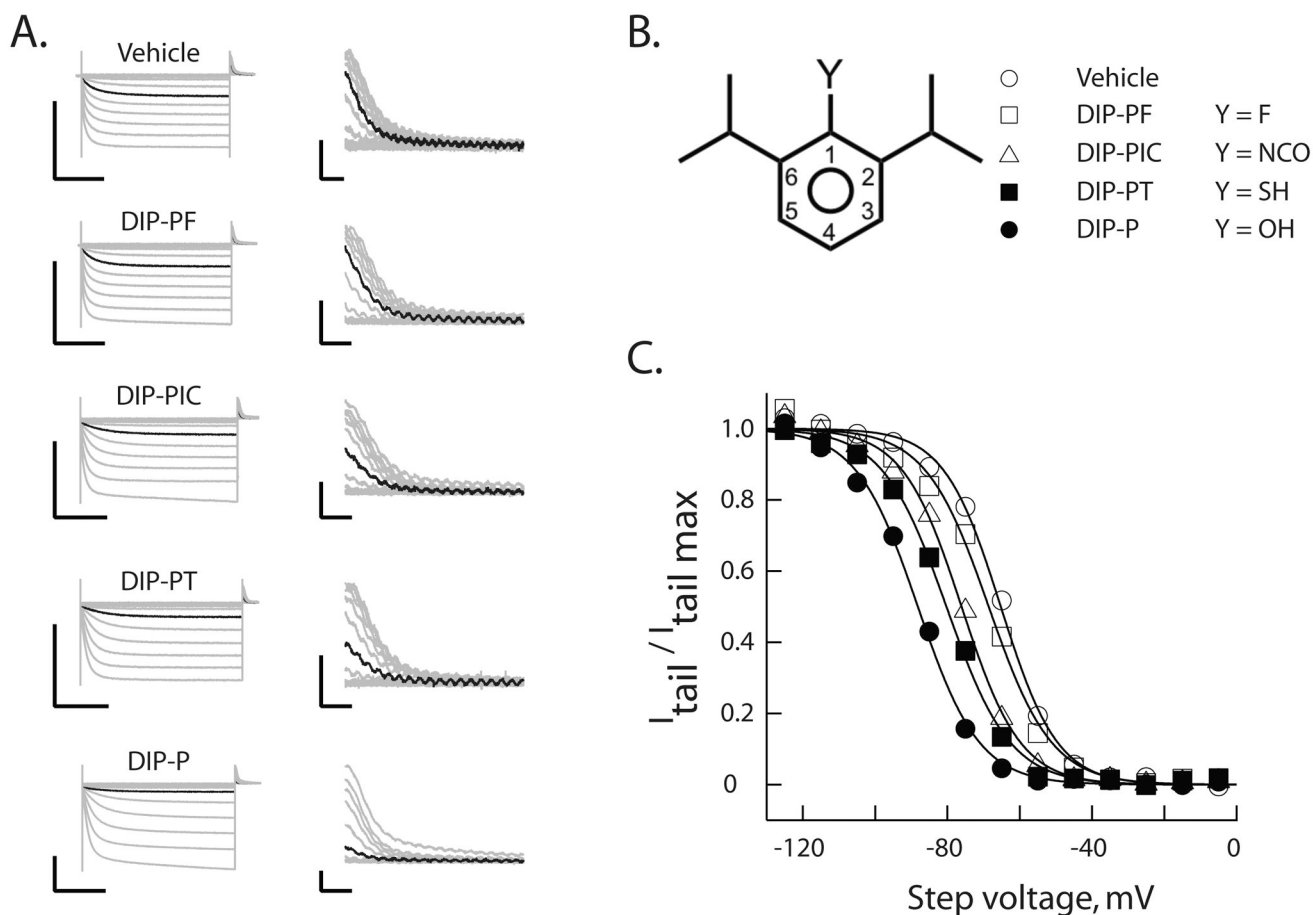
Figure 2: Hydrogen bond functionality at position 1 is important for alkylbenzene inhibition of HCN1 gating.

A. Representative voltage-clamp recordings of HCN1 currents (left) following incubation for 20 min in the absence or presence of 10 μM of the indicated reagent. Tail currents (right) are shown on expanded scales. In each case the black trace is the current recorded at an activation potential of −65 mV. To permit comparison, all recordings were obtained on the same day from distinct oocytes from a single donor frog. Scale bars are 2 μA and 1s (left) and 200 nA and 50 ms (right).

B. Schematic representation of 2,6-di-*iso*-propyl phenyls. Substitutions at the 1-position (as *per* the legend) describe molecules whose effects are reported in **A** and **C**.

C. Normalized steady-state activation curves constructed from the records shown in **A**. The smooth lines are fits of the Boltzmann function. Symbols represent molecules as described in **B**.
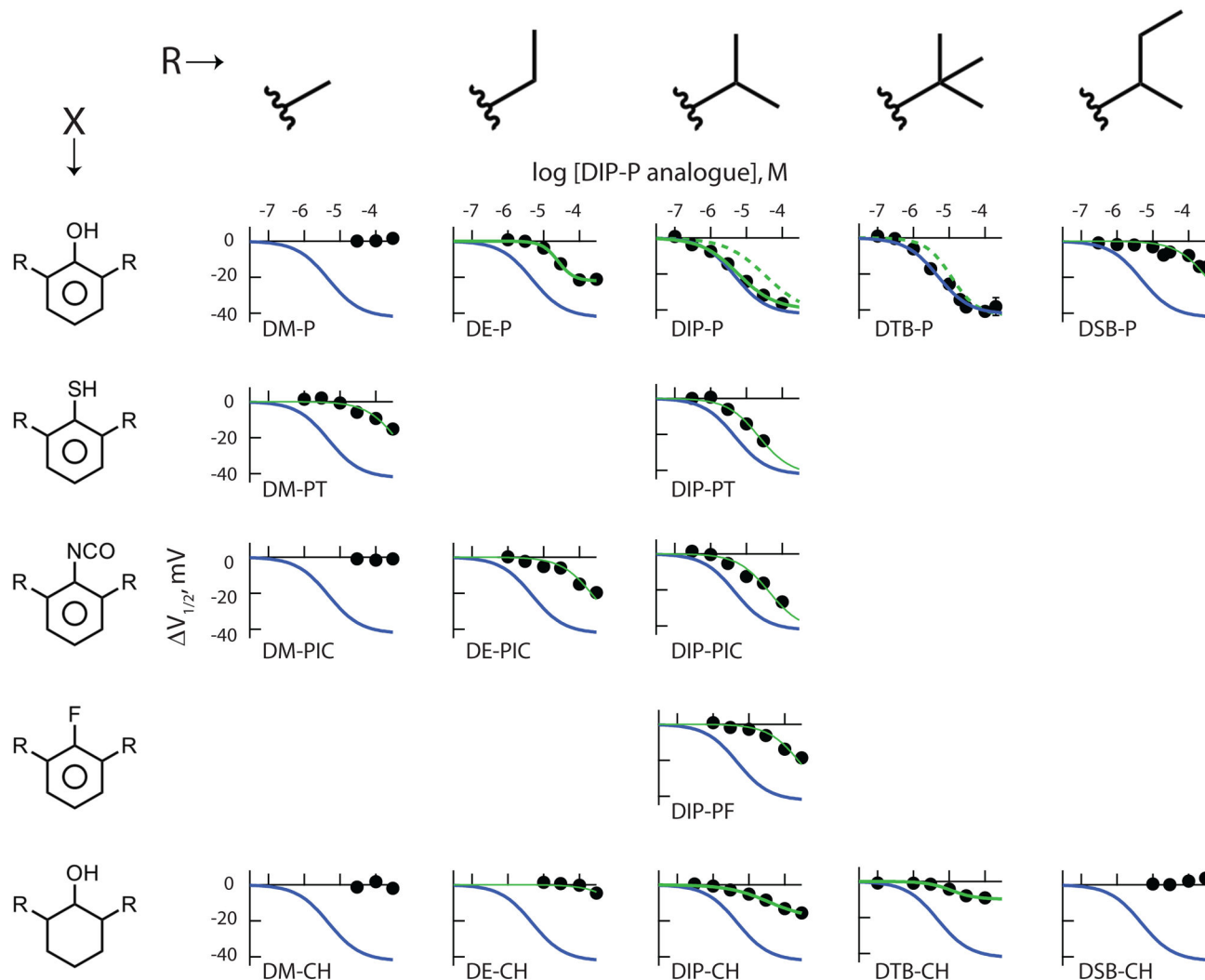
Figure 3: Inhibition by 2,6-di-alkyl phenyl derivatives reveals hydrogen bond potential, alkyl side chain identity and the presence or absence of π electrons (and/or ring planarity) all contribute to ligand association with HCN1 channels.

Panels show the shift in the $V_{1/2}$ as a function of concentration of each of the indicated ligands. Thick blue lines are the fit of the Hill equation to the DTB-P data, reproduced to facilitate visual comparison. Solid thick green lines are fits of the Hill function to ligands (other than DTB-P) that clearly demonstrated full (DIP-P) or partial (DE-P, DIP-CH, DTB-CH – see text and Figure 5) inverse agonist behavior. The dashed green lines in the DIP-P and DTB-P panels are scaled representations of the Hill fits to DIP-CH and DTB-CH, respectively with the cyclohexanol fit lines scaled according to the ratio $V_{1/2\ max}$ Phenol / $V_{1/2\ max}$ Cyclohexanol with all other terms of the cyclohexanol fit unaltered. The thin green lines are fits of the Hill equation to ligands whose efficacy is poorly determined (DM-PT, DE-PIC, DE-CH, DIP-PT, DIP-PIC, DIP-PF, DSB-P) wherein the $V_{1/2}$ max and h were held equal to the DTB-P values, with only the IC_{50} allowed to optimize. The number of independent determinations in each panel were: (phenols) 14, 44, 64, 165, 122; (thiols) 67, 45; (isocyanates) 15, 45, 47; (fluoro) 61; (cyclohexanols) 14, 25, 100, 53, 19.
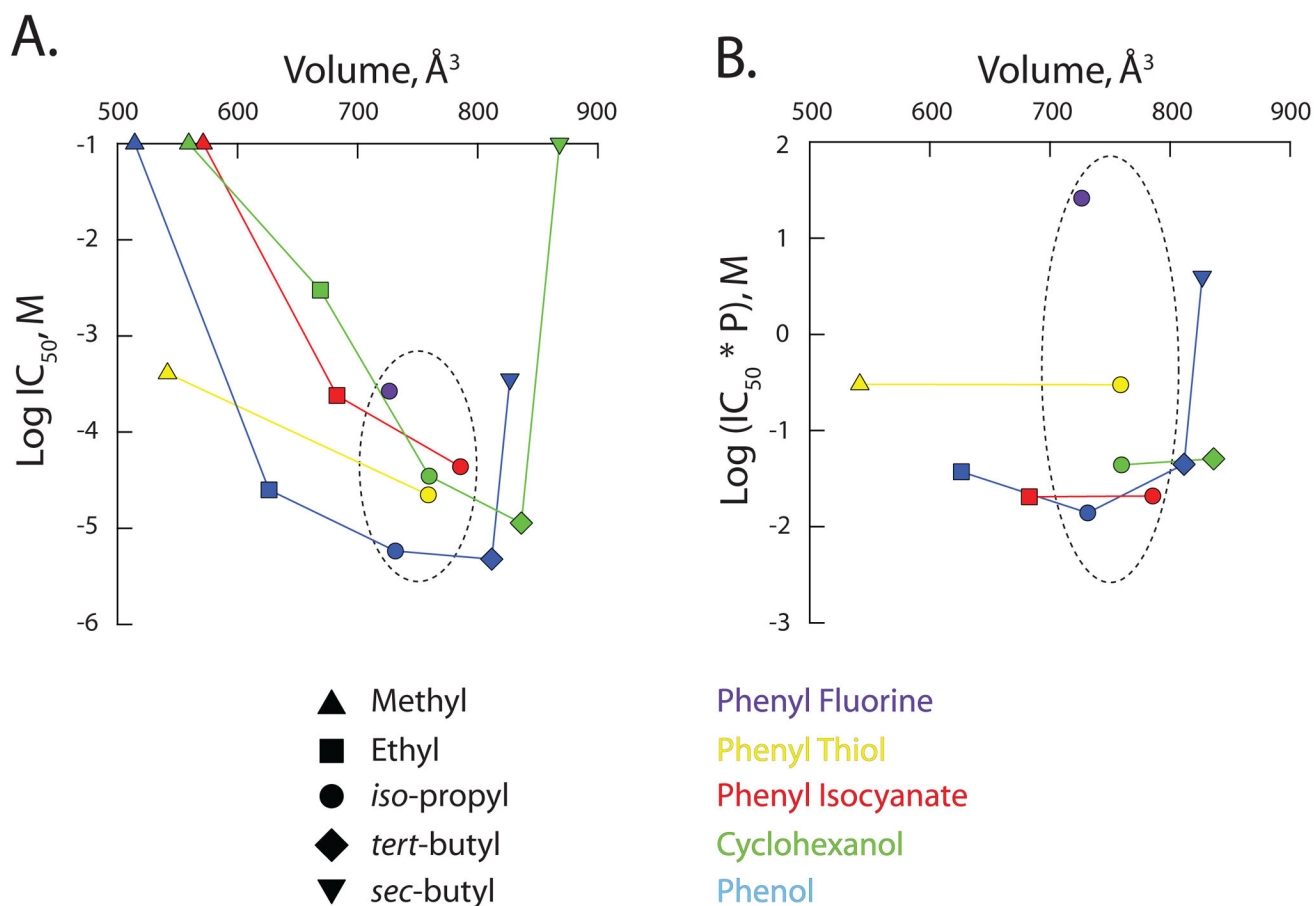
Figure 4: Inverse agonist potency of 2,6-di-alkyl phenyl analogues as a function of molecular volume.

The observed aqueous IC_{50} (**A**) and the partition-corrected IC_{50} (**B**) plotted as a function of the calculated molecular volume. Except where no inflection was observable in the concentration response curve, IC_{50}'s were determined from the fits shown in Figure 3 (see also Table 3). For ineffective molecules, the IC_{50} was set equal to 100 mM. The partition-corrected IC_{50} is the aqueous IC_{50} multiplied by the calculated partition coefficient, P (as *per* Tables 1 and 2). In both **A** and **B**, the dashed ellipse encircles the data for the *iso*-propyl family of reagents. As their IC_{50}s are at best ill-defined, values for DM-P (▲), DM-PIC (▲), DM-CH (▲), DE-CH (■) and DSBCH (▼) are omitted from **B**.
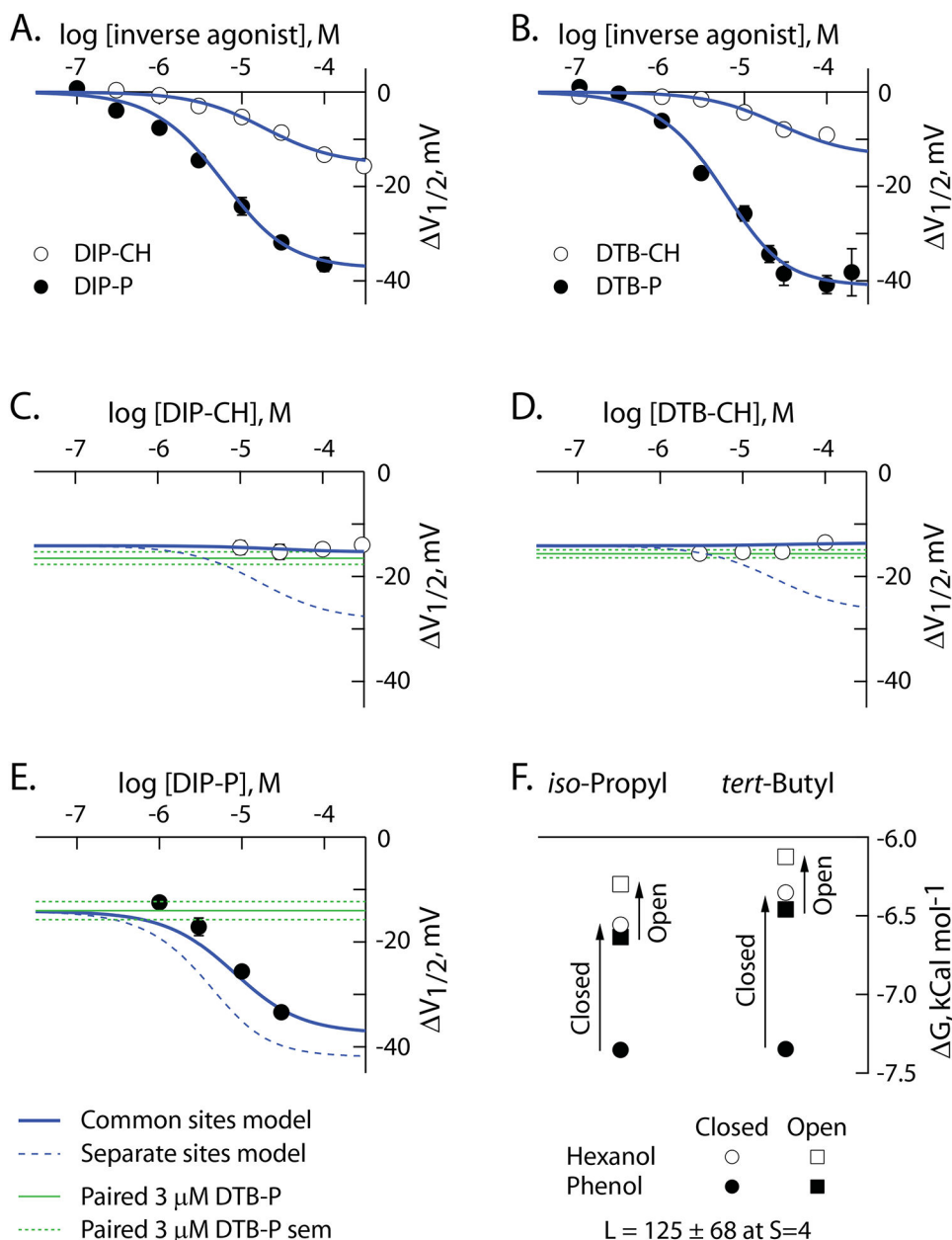
Figure 5: Alkylphenols and alkylcyclohexanols associate with HCN1 channels *via* four common, radially-distributed, sites.

A,B. $V_{1/2}$ as a function of concentration of *iso*-propyl (**A**) and *tert*-butyl (**B**) phenols and cyclohexanols. Data are reproduced from Figure 3. Solid blue lines are simultaneous fits of the common site model (S=4) to the data in these two panels and to the data in panels **C**-**E**.

C-E. $V_{1/2}$ as a function of concentration of DIP-CH (**C**), DTB-CH (**D**) or DIP-P (**E**), in the presence of 3 μM DTB-P. The solid blue lines are as defined in panels **A** and **B**. The dashed blue lines are the predicted behavior of the distinct site model at S=4 using the association constants determined from the fit of the common site model. The green lines report the mean value of $V_{1/2}$ (solid) and SEM (dashed) elicited by 3 μM DTB-P in paired controls for each

additivity condition. The number of independent determinations in **C**, **D** and **E** were 27, 80 and 33, respectively.

E. Association constants determined from the fits of the common site model with S=4 (as *per* **A**-**E** and reported in Table 4) transformed to free energy terms according to equation 6. The reported value of the opening equilibrium constant (L) is from this same fit.
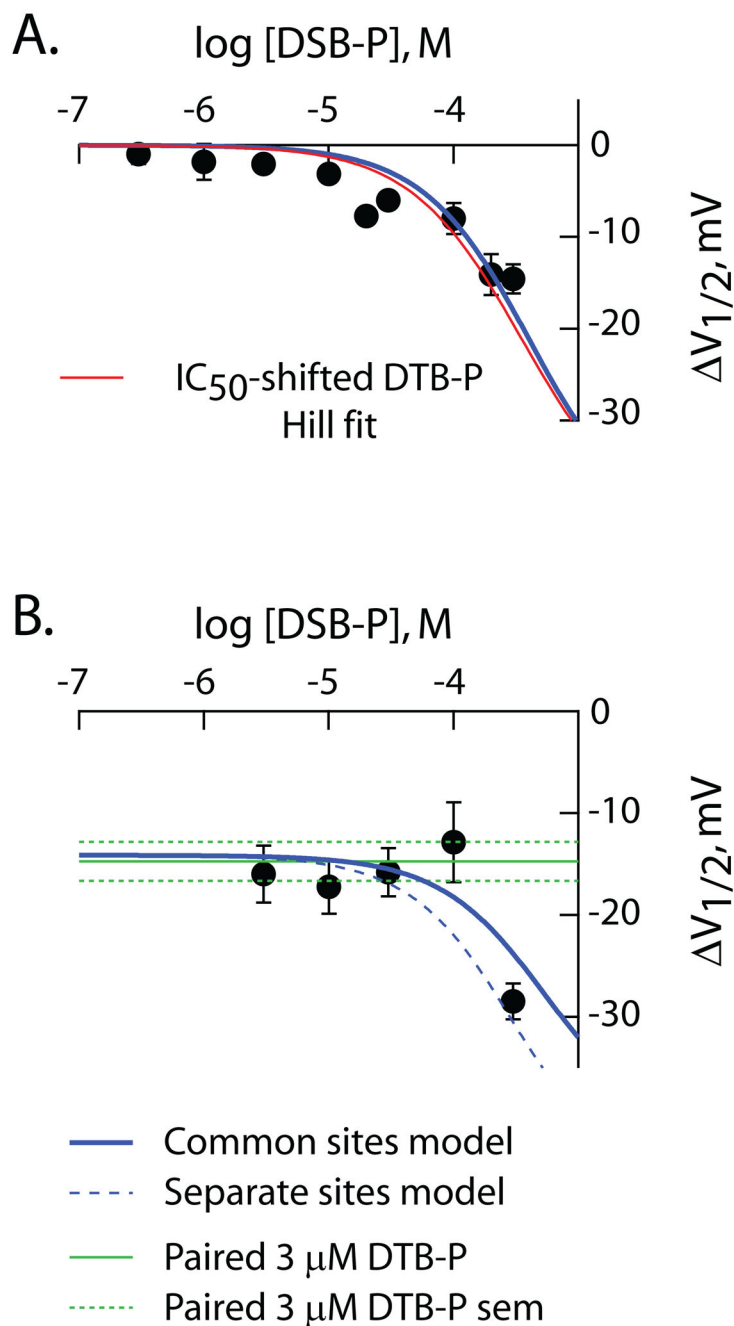
Figure 6: DSB-P is a low potency, high efficacy, inverse agonist.

$V_{1/2}$ as a function of concentration of DSB-P in the absence (**A**) and presence (**B**) of 3 μM DTB-P. Data in **A** are from Figure 3. The data in **B** are from 32 independent recordings. In both panels, the solid blue lines are simultaneous fits of the common site model (S=4) to the data in these two panels with all constants other than J_O^I and J_c^I held equal to the values determined in Figure 5 (see Table 4). J_O^I and J_c^I as determined from these fits were 881 ± 1,801 and 3,696 ± 2,948, respectively. The dashed blue line in **B** is the predicted behavior for the distinct site model at S=4 with parameters as described above. Discrete fits of the four models yielded χ^2 values of 165 and 167 (distinct site) and 600 and 128 (common site)

at S equal to 1 and 4, respectively. The symbols and red line in A are the observed $V_{1/2}$ for DSB-P and IC_{50}-adjusted DTB-P fit line (IC_{50} set to 355 μM) reproduced from the DSB-P panel of Figure 3. In **B**, the green lines report the mean value of $V_{1/2}$ (solid) and SEM (dashed) elicited by 3 μM DTB-P in paired controls.
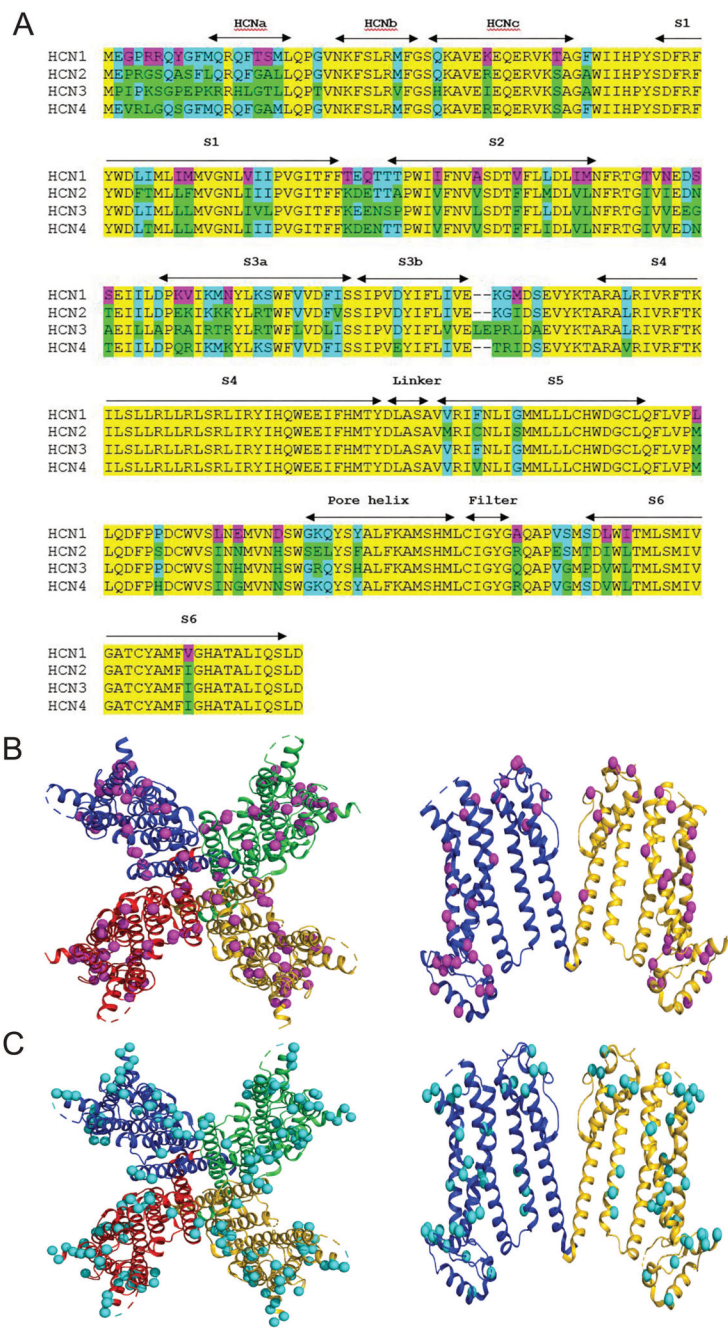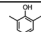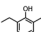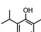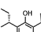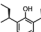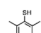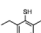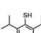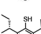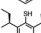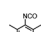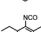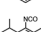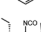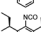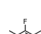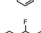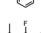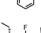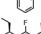
Figure 7: Cryo-EM structure of apo-state of alkylbenzene sensitive HCN1 channel core.
A. Amino acid sequence alignment for HCN1–4. Sequences shown are for the membrane embedded core region only, and correspond to mHCN1-ΔNΔC as previously described [25]. mHCN1-ΔNΔC contains 34 unique residues (with respect to mHCN2, hHCN3, and mHCN4) and 50 residues that are divergent from at least one other isoform. Magenta – residue identity unique to mHCN1; teal and green – locations where mHCN1-ΔNΔC diverges from at least one other isoform (teal shows commonality with mHCN1 while green highlights the divergent residue(s) in HCN2–4; yellow - four-fold conservation. Sequence alignment obtained using Clustal Omega(1.2.4) (https://www.ebi.ac.uk/Tools/msa/clustalo/)

for mouse (m)HCN1 (O88704.1), mHCN2 (O88703.1), human (h)HCN3 (Q9P1Z3.2), and mHCN4 (O70507.2).

B. Top-down (left panel) and side view (right panel) of the hHCN1 tetramer. As neither the divergent amino terminus nor the post-S6 C-terminus are involved in alkylbenzene inhibition of HCN1, these sequences have been eliminated from the structure for clarity. Note, the mouse and human HCN1 sequences are identical in the region defined by mHCN1-ΔNvΔC. HCN1 unique residues are shown as magenta spheres. Structure based on atomic coordinates of HCN1 in the unbound state from Lee & MacKinnon 2017 and deposited in the protein data bank (uniprot.org) under accession code 5U6O. In the right panel two of the opposing hHCN1 subunits removed for clarity.
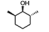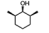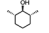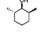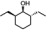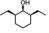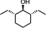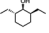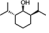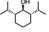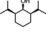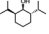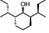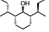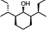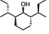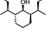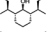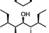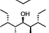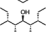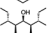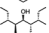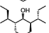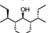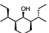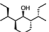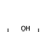
C. Top-down (left panel) and side-view (right panel) of hHCN1 as in **B** now showing the residues in mHCN1 that are common to at least one (but not all) other mHCN1 isoform (teal spheres).

Table 1:

Physicochemical properties of 2,6-di-alkyl substituted phenyls.

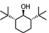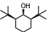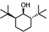| Abbreviation	Structure	MWt	Energy		Volume		H-Bonding		pKa		logP	
			kCal mol^{-1}	avg	Å^3	avg	D	A		avg		avg
DM-P		122.17	7.56		514.4		1	0.75	10.7±0.8		2.22	
DE-P		150.22	10.95		626.2		1	0.75	10.4±0.9		3.17	
DIP-P		178.27	17.40		731.5		1	0.75	11.1±1.1		3.38	
			18.25		832.8				10.7±1.5		4.08	
DSB-P		206.33	17.93	18.00	817.0	826.80	1	0.75	10.7±1.5	10.7±1.5	4.00	4.05
			17.82		830.5				10.7±1.5		4.06	
DTB-P		206.33	24.96		811.6		1	0.75	11.3±0.8		3.97	
DM-PT		138.23	25.58		541.7		0.8	0.5	7.2±2.2		2.87	
DE-PT		166.28	24.26		652.6		0.8	0.5	7.3±2.2		3.54	
DIP-PT		194.33	29.88		758.8		0.8	0.5	7.3±2.2		4.13	
			19.67		859.4				7.5±2.2		4.55	
DSB-PT		222.39	18.27	18.76	844.4	853.13	0.8	0.5	7.5±2.2	7.5±2.3	4.28	4.43
			18.32		855.6				7.5±2.2		4.46	
DTB-PT		222.39	56.16		846.2		0.8	0.5	7.3±2.2		4.17	
DM-PIC		147.18	15.22		571.4		0	3	n/a		1.49	
DE-PIC		175.23	19.81		682.8		0	3	n/a		1.93	
DIP-PIC		203.28	23.78		785.6		0	3	n/a		2.68	
			26.59		880.7				n/a		3.37	
DSB-PIC		231.34	26.59	26.59	880.4	880.61	0	3	n/a	n/a	3.35	3.36
			26.59		880.7				n/a		3.37	
DTB-PIC		231.34	43.32		865.1		0	3	n/a		2.91	
DM-PF		124.16	7.28		508.9		0	0	n/a		3.08	
DE-PF		152.21	11.29		622.1		0	0	n/a		3.82	
DIP-PF		180.27	14.49		726.3		0	0	n/a		4.99	
			16.90		835.2				n/a		5.79	
DSB-PF		208.32	15.36	15.93	813.5	827.61	0	0	n/a		5.46	5.67
			15.52		834.1				n/a		5.77	
DTB-PF		208.32	17.86		808.0		0	0	n/a		5.28	

H-bonding: D donor, A Acceptor; logP: log of the calculated octanol/water partition coefficient

Table 2:

Physicochemical properties of 2,6-di-alkyl substituted cyclohexanols.

Abbreviation	Structure	MWt	Energy kCal mol⁻¹	Energy avg	Volume Å³	Volume avg	H-Bonding D	H-Bonding A	pKa	pKa avg	logP	logP avg
			10.37		556.1				NR		1.98	
DM-CH		128.21	9.92	10.12	560.7	559.35	1	1.7	NR	NR	2.01	1.99
			9.80		563.8				NR		2.00	
			10.37		556.8				NR		1.98	
			12.87		665.5				NR		2.63	
DE-CH		156.27	11.86	12.51	670.2	668.87	1	1.7	NR	NR	2.71	2.66
			12.44		674.2				NR		2.69	
			12.87		665.5				NR		2.63	
			18.10		754.2				NR		3.06	
DIP-CH		184.32	15.96	17.12	762.1	759.50	1	1.7	NR	NR	3.10	3.10
			16.33		767.5				NR		3.17	
			18.10		754.1				NR		3.05	
			21.23		862.7				NR		3.77	
			18.35		871.7				NR		3.81	
			19.24		876.8				NR		3.87	
			21.03		862.0				NR		3.76	
			21.22		862.1				NR		3.76	
			18.44		870.5				NR		3.80	
			19.40		875.0				NR		3.86	
DSB-CH		212.38	21.22	20.06	861.3	868.08	1	1.7	NR	NR	3.76	3.80
			21.16		863.1				NR		3.77	
			18.30		872.3				NR		3.82	
			20.24		876.8				NR		3.87	
			21.09		862.6				NR		3.77	
			21.12		862.7				NR		3.77	
			18.35		871.5				NR		3.81	
			19.34		876.6				NR		3.87	
			21.23		861.7				NR		3.76	
			29.03		829.8				NR		3.56	
			27.87		841.9				NR		3.76	
DTB-CH		212.38	23.71	27.41	843.9	836.34	1	1.7	NR	NR	3.73	3.65
			29.03		829.8				NR		3.56	

H-bonding: D donor, A Acceptor; logP: log of the calculated octanol/water partition coefficient

Table 3:

Hill equation parameters.

Ligand	Hill Fit Paramters (mean ± SD)		
	IC$_{50}$, µM	V$_{1/2}$ max, mV	h
DM-PT	408 ± 55	--	--
DE-P	25.1 ±2.7	−22.1 ± 1.0	1.95 ± 0.44
DE-PIC	240 ± 20	--	--
DE-CH	2995 ± 723	--	--
DIP-P	5.8 ± 1.2	−39.8 ± 2.3	0.85 ± 0.11
DIP-PT	22.2 ± 1.8	--	--
DIP-PIC	43.7 ± 3.8	--	--
DIP-PF	267 ± 24	--	--
DIP-CH	35.0 ± 21.0	−18.9 ± 3.4	0.76 ± 0.19
DTB-P	4.8 ± 0.8	−42.4 ± 2.8	0.97 ± 0.13
DTB-CH	11.4 ± 4.2	−9.9 ± 1.5	1.28 ± 0.47
DSB-P	355 ± 38	--	--

Where not reported, parameters were constrained to those determined for DTB-P as described in Section 2.3 and Figure 3. For all ligands, fitted parameters were significantly different from those of DTB-P and DIP-P ($P < 0.05$: one-way ANOVA).

Table 4:

Model determined association constants for phenol and cyclohexanol binding to HCN1 channels.

Constant	DTB-P	DTB-CH	Fold Change
K_C	24.6 ± 4.5	4.6 ± 2.0	5.4
K_O	5.5 ± 2.6	3.1 ± 1.5	1.8
Constant	**DIP-P**	**DIP-CH**	**Fold Change**
Q_C	24.8 ± 4.4	6.5 ± 2.2	3.8
Q_o	7.4 ± 2.1	4.2 ± 1.5	1.8
Constant	**DSB-P**	**DSB-CH**	**Fold Change**
J_C	0.4 ± 0.3	*no effect*	--
J_O	0.1 ± 0.2	*no effect*	--

Constants and their errors have been divided by 10^4 for clarity.